The Plant Cell, Vol. 29: 207–228, February 2017, www.plantcell.org © 2017 American Society of Plant Biologists. All rights reserved.

LARGE-SCALE BIOLOGY ARTICLE

Protein Degradation Rate in *Arabidopsis thaliana* Leaf Growth and Development[OPEN]

Lei Li, Clark J. Nelson, Josua Trösch, Ian Castleden, Shaobai Huang, and A. Harvey Millar[1]

ARC Centre of Excellence in Plant Energy Biology, University of Western Australia, Crawley 6009, Western Australia, Australia

ORCID IDs: 0000-0003-1508-5484 (L.L.); 0000-0002-7770-7333 (J.T.); 0000-0003-3667-611X (S.H.); 0000-0001-9679-1473 (A.H.M.)

We applied ^{15}N labeling approaches to leaves of the *Arabidopsis thaliana* rosette to characterize their protein degradation rate and understand its determinants. The progressive labeling of new peptides with ^{15}N and measuring the decrease in the abundance of >60,000 existing peptides over time allowed us to define the degradation rate of 1228 proteins in vivo. We show that Arabidopsis protein half-lives vary from several hours to several months based on the exponential constant of the decay rate for each protein. This rate was calculated from the relative isotope abundance of each peptide and the fold change in protein abundance during growth. Protein complex membership and specific protein domains were found to be strong predictors of degradation rate, while N-end amino acid, hydrophobicity, or aggregation propensity of proteins were not. We discovered rapidly degrading subunits in a variety of protein complexes in plastids and identified the set of plant proteins whose degradation rate changed in different leaves of the rosette and correlated with leaf growth rate. From this information, we have calculated the protein turnover energy costs in different leaves and their key determinants within the proteome.

INTRODUCTION

For plants to respond to the daily requirements of cellular maintenance and for their organs to progress through different developmental stages, new complements of proteins need to be synthesized while existing ones are degraded. Protein synthesis occurs via ribosomes in the cytosol, plastid, and mitochondrion. Synthesis rate is defined by the abundance and availability of different mRNA (Juntawong et al., 2014), the energetic status of cells to provide the amino acids and ATP for catalysis (Edwards et al., 2012), and the posttranslational regulation of ribosomal function (Ren et al., 2011). Cellular protein degradation is achieved by the coordinated action of the proteasome on ubiquitinated proteins in the cytosol (Vierstra, 2009), autophagy of cytosolic complexes and organelles through vacuole-based protein degradation machinery (Araújo et al., 2011), and a network of organelle-localized proteases (Janska et al., 2013; van Wijk, 2015). The rates of synthesis and degradation of individual proteins define the proteomes of plant tissues and their rate of change.

The combination of protein synthesis and degradation is often termed protein turnover; however, there are many different definitions and assumptions made in using this term and in calculating it. Protein degradation rates and calculated turnover rates can be measured on a total plant protein basis by combining all polypeptides as a group and measuring rates at which "old protein" disappears or "new protein" replaces old. These types of calculation look at the amount of original protein remaining and/or the proportion of new protein to old at several time points and calculate a rate of renewal. This approach typically does not consider the inherent rate of degradation of the newly synthesized material. Rates calculated without considering degradation of new proteins are intrinsically linked to the growth rate of the tissue which can dramatically alter the pool size of the new protein component over time. Protein turnover of roots has been measured this way using pulse chase ^{14}C-leucine labeling of fast- and slow-growing grass species (Scheurwater et al., 2000) to define degradation rates of 0.12 to 0.16 d^{-1} and a total protein half-life of 4 to 6 d. Using *Arabidopsis thaliana* rosettes and $^{13}CO_2$ pulse-chase labeling (and a focus on the relative isotope ratio of Ala residues) degradation rates of 0.03 to 0.04 d^{-1} and a leaf protein half-life of 3.5 d were calculated by combining degradation and original protein dilution through new protein synthesis (Ishihara et al., 2015).

Protein degradation and turnover can also be measured for specific proteins of interest. This requires a method to identify individual proteins and to differentiate between old and new polypeptides for the same protein over the timeframe of measurement. Early studies used antibodies and generic protein biosynthesis inhibitors to do this, but given the cellular consequence of protein biosynthesis inhibition, there are many pleiotropic effects in such measurements in all but very short timeframes (Vögtle et al., 2009; Armbruster et al., 2010). The combination of stable isotopes and peptide mass spectrometry have recently allowed old and new protein populations to be differentiated without the need for protein biosynthesis inhibition and have become a method of choice in new studies. The experimental measurement of protein degradation rate (K_D) through isotopic labeling and mass spectrometry (MS) has enabled data sets of hundreds of individual protein degradation rates and half-lives to

[1] Address correspondence to harvey.millar@uwa.edu.au.
The author responsible for distribution of materials integral to the findings presented in this article in accordance with the policy described in the Instructions for Authors (www.plantcell.org) is: A. Harvey Millar (harvey.millar@uwa.edu.au).
[OPEN]Articles can be viewed without a subscription.
www.plantcell.org/cgi/doi/10.1105/tpc.16.00768

Downloaded from https://academic.oup.com/plcell/article/29/2/207/6099059 by guest on 20 August 2022

be assessed in yeast, mammalian cell culture, and intact animals typically using single labeled amino acids (SILAC) (Price et al., 2010; Schwanhäusser et al., 2011; Yip et al., 2011). Plants are typically not amenable to successful SILAC labeling due to their synthesis and interconversion of all protein amino acids. As a result, studies have assessed the utility of various metabolic labels (^{2}H, ^{13}C, and ^{15}N) for the purpose in plants (Yang et al., 2010; Chen et al., 2011; Li et al., 2012). Recently, metabolic labeling with inorganic ^{15}N has been the most commonly used stable isotope incorporation technique to define degradation or turnover rates of organelle proteins in Arabidopsis cell culture (Nelson et al., 2013), protease targets in Arabidopsis leaf mitochondria (Huang et al., 2015; Li et al., 2016), ~500 proteins in barley (*Hordeum vulgare*) leaves (Nelson et al., 2014), ~200 membrane and microsomal fraction proteins from Arabidopsis roots (Fan et al., 2016), and ~500 *Medicago truncatula* leaf and root proteins during drought and recovery from drought (Lyon et al., 2016). One study has also followed selected protein degradation rates using $^{13}CO_2$ in Arabidopsis leaves (Ishihara et al., 2015). While the primary data from labeling in each case represent relative isotope abundance for a given peptide, different methods have been used to calculate protein degradation, synthesis, and turnover rates and protein half-lives. Some of these calculations considered the growth rate of tissues, the degradation rate of newly synthesized proteins, and the relative abundance of different proteins during labeling, while others did not. Depending on the method used, the K_D reported can be highly dependent on tissue growth rate and/or on relative abundance of the protein over time and may not represent a property of the polypeptide per se. As a result, we still have limited data on the rate of protein degradation for different classes of plant proteins and little clarity about whether degradation rate is a variable or constant feature of the lifecycle of a specific plant polypeptide type.

Here, we aimed to define the key features of proteins that determine their experimental degradation rate and measure changes in these rates for given protein sets at different stages of Arabidopsis leaf growth through assembly of a larger and more precise data set than used in previous studies. This approach provides a foundational data set for protein degradation rates in Arabidopsis and evidence of which proteins have variable degradation rates as leaves grow. In the process, we have identified rapidly degrading subunits in a variety of protein complexes in plastids, found the set of proteins for which degradation rate positively or negatively correlates with leaf growth rate, and considered the protein turnover energy costs for total and specific proteins in different leaves of the Arabidopsis rosette.

RESULTS

Changes in Arabidopsis Leaf Protein Content at Different Stages of Leaf Development

When specific proteins remain in steady state within the proteome over the time course of ^{15}N progressive labeling, a single dilution effect can be calculated and applied to account for the rate of tissue growth. To calculate this dilution effect, Arabidopsis seedlings were grown in natural abundance hydroponic culture medium (99.6% ^{14}N) for 21 d until they produced their tenth true leaf, a stage referred to as leaf production stage 1.10 (Boyes et al., 2001). To compare their total protein abundance, leaf numbers 3, 5, and 7 from a series of rosettes were collected over a period of 5 d (Supplemental Figure 1A). Proteins were extracted from these leaf samples for analysis of total leaf protein content (Figure 1). This allowed an assessment of the growth rate of different leaves of the rosette on a protein basis. We assessed protein content by protein extraction and amido black measurement (Supplemental Data Set 1) and by imaging gel-separated proteins from whole leaves ground into sample buffer (Supplemental Figure 1B and Supplemental Data Set 1). Leaf 3 increased its total protein content by only 3% per day, in contrast to leaves 5 and 7, which grew at 3 and 5 times this rate, respectively (Figure 1). As a consequence, leaf 7 nearly doubled in size and total protein content over five days while leaf 3 hardly grew at all.

Protein Degradation Rate of Specific Proteins in Arabidopsis Leaves

Leaves in the Arabidopsis rosette were then sampled at the same time points as above, but in this case the hydroponic medium was changed at T = 0 from 99.6% ^{14}N to 98% ^{15}N to allow progressive labeling of each leaf over the time course of 5 d. A flow diagram of the experiment and the sample preparation for mass spectrometry

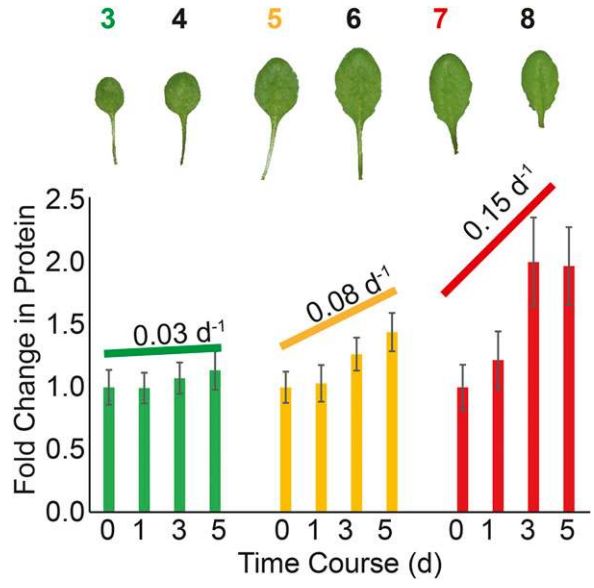

Figure 1. Individual Growth Rates of Leaves in the Arabidopsis Rosette and the Consequent Fold Change in Protein over Time.

Leaves 3, 5, and 7 from Arabidopsis plants grown in hydroponic culture were collected over a time course (T0, 1, 3, and 5 d) beginning with 21-d-old plants that had developed 10 leaves (leaf production stage 1.10). Typical images of leaves 3 to 8 from these plants at the beginning of the experiment are shown. The growth of leaves over the subsequent 5 d were determined by following the fold change in protein per leaf at each time point compared with T0 for leaf 3 (green), leaf 5 (yellow), and leaf 7 (red). An average relative growth rate (d^{-1}) was determined from both changes in fresh weight and protein content by scanning images of gels (Supplemental Figure 1 and Supplemental Data Set 1).

Downloaded from https://academic.oup.com/plcell/article/29/2/207/6099059 by guest on 20 August 2022

are shown in Supplemental Figure 2. Extensive liquid chromatography-tandem MS analysis of these samples provided data from 61,196 independently quantified peptides for which we could acquire the ratio between natural abundance (NA) and heavy (H) labeled peptides. Using the ratio of labeled to NA peptides and fold change in protein (FCP) as each leaf grew (Figure 1), we estimated degradation rate for 1228 nonredundant Arabidopsis proteins. Inclusion in this list required each protein to be quantified in ≥3 of 27 samples, the number of peptides quantified independently in the 27 samples to be greater or equal to 5 and for the protein identification to be $P > 0.95$ as outlined in Methods (Supplemental Data Sets 2A and 2B). Sample calculations of labeled protein fraction [LPF; i.e., H/(H+NA)] are shown for a slow degrading peptide (Supplemental Figure 3A) and a fast degrading peptide (Supplemental Figure 3B) in each of the three leaves over the time course. The degradation rates (K_D) of 1228 proteins were calculated as explained in the Methods section and as shown in Supplemental Figure 3C for the example of a fast and a slow degrading peptide. K_D is the proportional decrease of the current protein abundance per day; i.e., it is the exponential constant of the decay rate for each protein and as such has units of d^{-1}. These K_D rates showed a wide distribution ranging from 0 to 2 d^{-1}, which is equivalent to half-lives for proteins of several hours to several months. These are the average K_D across all cell types in a leaf tissue examined and, like all quantitative proteomics, any cell type-specific differences will be lost in this averaging. The median relative SE (RSE) was <10% for measurement of K_D of a specific protein (Supplemental Data Set 2B). In general, ~15% of the data (184 proteins) showed degradation rates more than 2 times the K_D median (~0.22 d^{-1}), which we defined as relatively fast degrading proteins; ~13% (161 proteins) showed degradation rates of less than half the median (~0.055 d^{-1}), which we defined as relatively slowly degrading proteins, while the majority (72%) showed values in the 4-fold range between these K_D values (Supplemental Data Set 2B).

Determination of the fraction of proteins that are labeled, represented by the LPF value, is a binary differentiation between two populations of peptides. As the peptides measured typically contained 8 to 30 nitrogen atoms per peptide, only a few nitrogen atoms anywhere in the peptide would place a peptide in the heavy-labeled pool. All such peptides were considered heavy-labeled and the degree of ^{15}N labeling formed no part of our calculations. This is distinct from measurements of the incorporation of a specific amino acid within a peptide, which requires a detailed knowledge of the peptide incorporation ratio in that amino acids and the free amino acid pool incorporation ratio to calculate peptide synthesis levels (Ishihara et al., 2015). However, despite these advantages, the LPF approach employed here can be affected by a lag before new protein synthesis can be effectively distinguishable from previously present (NA) proteins. The lag is overcome as soon as a 10 to 15% labeling level is reached in major amino acid pools (Nelson et al., 2014). The three different leaves did show some differences in ^{15}N labeling efficiency (Supplemental Figure 4). A regression method can be used to determine the lag effect as the lag in the x-intercept value when graphing of all time points (Nelson et al., 2014). Calculations based on this method showed leaves 3, 5, and 7 had a 5- to 6-h lag before ^{15}N reached this 10 to 15% threshold (L3 = 4.7 h, L5 = 5.9 h, and L7 = 5.2 h). This represented 4 to 25% of the time interval for day 5, day 3, and day 1 data, respectively, which was similar to the RSE of our calculations for any one protein. To examine if this calculable lag would systematically effect K_D values, we selected 146 proteins that were quantified in all samples at all time points and plotted their degradation rates together across all three replicates, time points, and leaf types. No significant trends were apparent to indicate that this general effect would bias our data (Supplemental Figure 5). We are not aware of literature that has divided leaves into cell types to show differences in ^{15}N incorporation rate within leaves to justify the concern that lag averages are not a fair reflection for an average leaf calculation.

Grouping proteins by their functional category (Figure 2A) showed that most protein groups maintained the median degradation rate of ~0.11 d^{-1}. Exceptions were proteins involved in protein synthesis that degraded at closer to 0.03 d^{-1} and stress, secondary metabolism, and redox proteins that degraded at rates approaching 0.20 d^{-1}. Individual proteins degrading at very high rates were found in many functional categories and typically showed rates from 0.6 up to 2.0 d^{-1}, which was 6 to 20 times the median K_D and 4 to 13 standard deviations from the median (Figure 2A). The 20 fastest degrading proteins comprised a set of eight plastid proteins, six cytosolic proteins, and six proteins localized elsewhere in the cell (Table 1). To look for evidence of differences in the rate of autophagy of cellular structures or the role of intra-organellar proteases in changing the degradation rate inside specific organelles, we arranged the data set into the final subcellular location of proteins using the location Bayesian classifier, SUBAcon (Tanz et al., 2013; Hooper et al., 2014). This showed a lower median degradation rate of mitochondrial, plastidial, and nuclear proteomes and a higher median degradation rate for the proteomes of endoplasmic reticulum (ER) and the Golgi apparatus. This is broadly consistent with the physical separation of organelle proteomes from the cytosolic proteolysis system and the transient nature of the protein complement of ER and Golgi (Figure 2B). Direct comparison of protein degradation rates in this data set to either orthologs in barley (Nelson et al., 2014) was possible because the same measurement approach was used in both of these studies (Figure 2C). This comparison showed that four ortholog pairs between the two species had consistently high degradation rates, namely, the thiamin synthesis enzymes THI1 and THIC, D1 of PSII, and PTERIN DEHYDRATASE ($R = 0.99$). However, more broadly this comparison showed a relatively low correlation between degradation rate of the majority of Arabidopsis and barley homologous pairs ($R = 0.38$).

Changes in Arabidopsis Leaf Proteomes at Different Stages of Development and across the Diurnal Cycle

To check if proteins remained in steady state within leaf proteomes over the time course of our measurements, the relative abundances of specific Arabidopsis proteins were assessed in the samples from different time points by spiking natural abundance samples after protein extraction with a ^{15}N fully labeled protein sample from a separate batch of Arabidopsis leaves kept as a reference standard. Mixed proteins were then in-solution digested by trypsin for MS analysis. A flow diagram of this experiment and the sample preparation for MS are also shown in

Downloaded from https://academic.oup.com/plcell/article/29/2/207/6099059 by guest on 20 August 2022

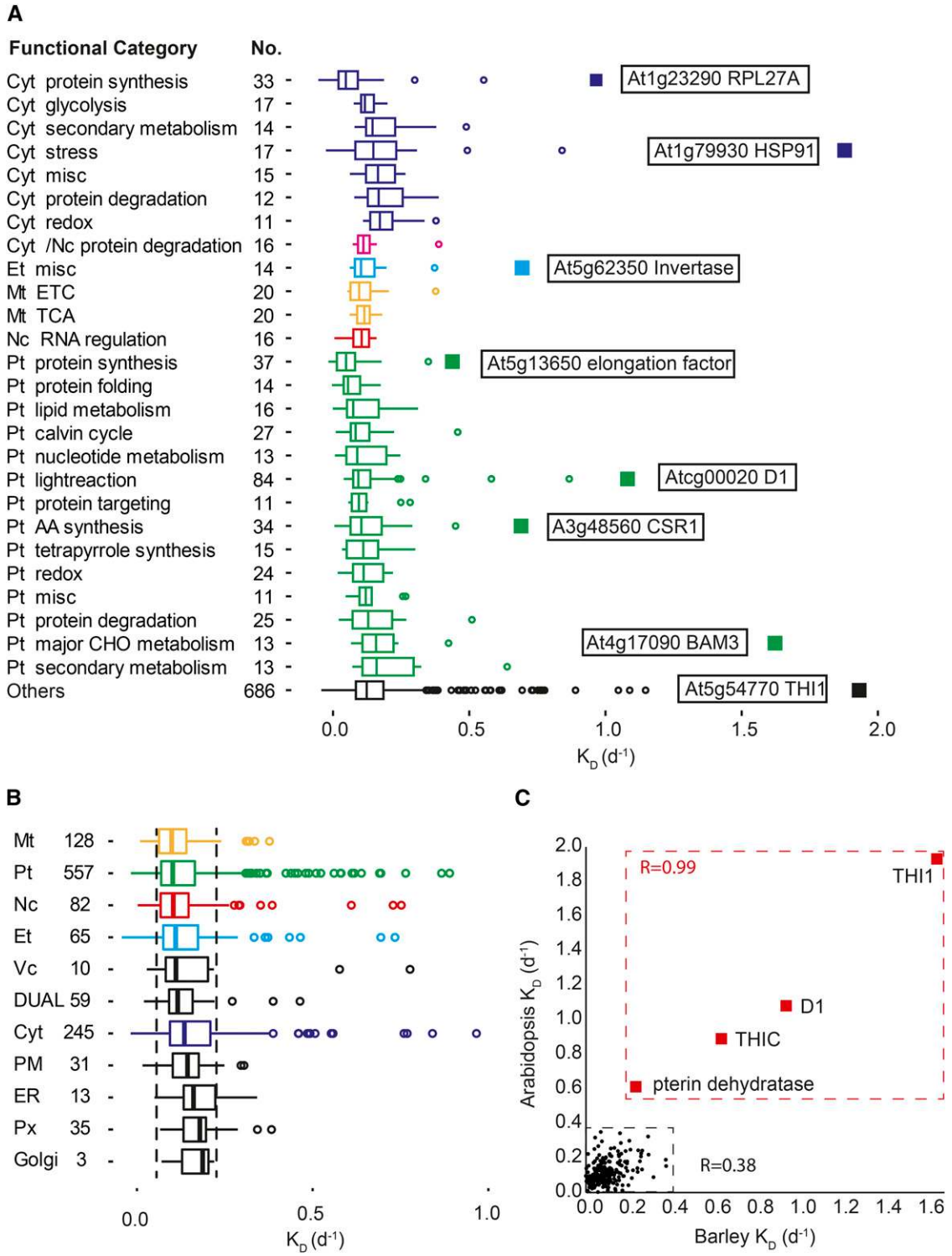

Figure 2. Degradation Rates of 1228 Arabidopsis Proteins Reported as Averages Based on Functional Categories or Localization inside Cells and in Comparison to Barley Orthologs.

(A) Average Arabidopsis leaf protein degradation rates box-plotted by functional categories and their localization in cells. Functional categories were acquired from MapCave and localization information from SUBAIII. Only major functional categories and localization groups ($n > 10$) are shown. Median, quartiles, and standard deviations are shown. Outliers are shown as hollow dots and extreme outliers are highlighted as solid squares and annotated. The five

Downloaded from https://academic.oup.com/plcell/article/29/2/207/6099059 by guest on 20 August 2022

Supplemental Figure 2. This provided quantitation of 1697 nonredundant proteins. Proteins were included in this group if they were quantified in ≥3 of 36 samples, the number of peptides quantified independently in the 36 samples was ≥5, and the protein identification had P > 0.95 as outlined in Methods (Supplemental Data Set 3A). In total, 955 proteins in this set of 1697 were also found in the set of 1228 proteins for which we calculated a K_D value (Figure 3A; Supplemental Data Set 3B). Principal component analysis of protein relative abundance data from this MS experiment showed that the three different leaves in the rosette could be separated by a single principal component explaining 43% of the variation (Figure 3B). Only minor variations were observed in the principal component analysis between samples of the same leaf number at different points in time. Changes in relative protein abundances over time in the different leaf proteomes were compared and statistically evaluated by *t* tests and one-way ANOVA (Figure 3C; Supplemental Data Set 3C). This analysis indicated that only a few percent of proteins significantly changed in abundance in leaf 3 across the whole time course, which was close to expectation for random variation in the experiment (P < 0.01). Leaf 7 showed a similar pattern of percentage differences with only the samples from the day 1 showing significant differences from day 5 samples. No specific proteins were found to change in abundance between all time points in leaf 3 and leaf 7 (Figure 3C). By contrast, leaf 5 showed 13 to 33% of the analyzed protein set differing in relative abundance by day 5; however, only 0.4% (two proteins) showed consistent changes across the time course (Supplemental Data Set 3C). This revealed that relatively high abundance proteins of leaf 3 and leaf 7 were effectively in steady state during the experiment, albeit with different rates of new tissue growth (Figure 1); thus, steady state principles could be applied to establish protein degradation rates for existing proteins in leaves 3 and 7 over a 5-d period. For leaf 5, some variation in abundance was evident but only at the day 5 time point. The majority of data showed only 20 to 30% changes in abundance, for the proteins that differed at day 5, which will not have a major effect on K_D calculations.

One important factor that could explain the need for rapid degradation of some proteins is a circadian or diurnal change in transcription and translation that would need to be matched by the degradation rate to enable a daily rhythm in protein abundance. Expression profiling of Arabidopsis leaves has previously shown that diurnal patterns of transcription can underlie daily fluctuations in protein abundances in leaves (Mockler et al., 2007; Giraud et al., 2010; Lee et al., 2010). To test if enhanced degradation rate correlates with diurnal gene expression or protein abundance changes, we attempted to correlate the calculated K_D with the degree of change in transcript abundance of diurnally regulated genes (Mockler et al., 2007) or the degree of change in Arabidopsis protein abundance following 8 h of illumination (Liang et al., 2016); however, we found no significant correlation of these with K_D (R = 0.01 and R = 0.02–0.08; n = 917 and 1158, respectively). By contrast, when the 1228 K_D values were separated into slow (n = 161), intermediate (n = 883), and fast (n = 184) groups, as outlined above, and compared with light-induced, dark-induced, and nondiurnal transcripts (as defined in Mockler et al., 2007), nonparametric tests showed an enrichment (P < 0.01) of light-induced transcripts in the fast K_D group compared with the nondiurnal or dark-induced transcripts. This apparent link between light-induced diurnal expression and fast K_D was observed in long-day or 12 h/12 h experiments in both Col-0 and L*er* backgrounds (Smith et al., 2004; Bläsing et al., 2005; Mockler et al., 2007).

Intrinsic Protein Properties Linked to Degradation Rate

The fact that protein degradation rate of individual proteins was quite reproducible between leaf types over the time course indicated that some factors intrinsic to each protein's expression, protein properties, or susceptibility to modification, unfolding, or proteolysis could be a central controller of protein degradation rate. The N-end rule proposes that the N-terminal amino acid of a protein is a key driver for turnover rate. A series of stabilizing and destabilizing N-terminal amino acids have already been experimentally defined in yeast and mammals (Bachmair et al., 1986; Gonda et al., 1989). However, we were unable to find any statistical linkage between K_D and either the N-end amino acid of mature proteins or sets of amino acids considered to be stable, unstable, or of average stability based on yeast and mammalian data (Figure 4A; Supplemental Data Set 4A). Amino acid residues within protein sequences can promote ordered aggregation, which can be a precondition for altered rates of protein degradation in mammals. The TANGO algorithm can predict this aggregation propensity (Fernandez-Escamilla et al., 2004). In our set of 1228 proteins, the top 100 fastest degrading proteins show significantly higher protein aggregation propensity (AGG; P < 0.05) and longer amino acid length (LEN; P < 0.05), but no significant difference (P = 0.70) in AGG/LEN when compared with the 100 slowest turnover proteins (Figure 4B; Supplemental Data Set 4B). This result implies that the aggregation propensity of faster degradation proteins in Arabidopsis was dependent on length and there was a tendency for proteins to be longer in the set of faster degrading proteins. Integral membrane proteins require different machinery for degradation than soluble proteins and have different accessibility to proteases (Fleig et al., 2012; Avci and

Figure 2. (continued).

major localizations are highlighted with colors: cytosol (Cyt, blue), nucleus (Nc, red), extracellular (Et, cyan), mitochondrion (Mt, yellow), and plastid (Pt, green).

(B) Protein degradation rates of the 1228 proteins box-plotted based on localization within the cell. DUAL, dual targeting proteins; Vc, vacuole; PM, plasma membrane; Px, peroxisomal. Other abbreviations as in **(A)**.

(C) Protein degradation rates of a subset of 288 Arabidopsis proteins for which orthologs in barley had published rates. One spot represents a protein turnover rate in barley (*x* axis) and Arabidopsis (*y* axis). Four outliers (2 SD above median, in red dashed line rectangle) are shown (Pearson correlation, R = 0.99). The remaining 284 proteins (pointed out by black dashed line rectangle) are shown by black dots (Pearson correlation, R = 0.38).

Downloaded from https://academic.oup.com/plcell/article/29/2/207/6099059 by guest on 20 August 2022

Table 1. The 20 Most Rapidly Degrading Proteins in Arabidopsis Leaves

Protein		Location	Functional Category	K_D (d^{-1})	SE	Brep No.	Pep No.	Half-Life (d)
At5g54770	THI1	Plastid	Cofactor and vitamin metabolism	1.93	0.16	12	31	0.36
At1g79930	HSP91	Cytosol	Stress	1.88	0.49	6	6	0.37
At4g17090	BAM3	Plastid	Major CHO metabolism	1.62	0.11	7	12	0.43
At3g19710	BCAT4	Cytosol	Amino acid synthesis	1.15	0.09	5	8	0.60
At3g22200	POP2	Mito	Amino acid synthesis	1.09	0.31	4	5	0.64
AtCg00020	D1	Plastid	Light reaction	1.08	0.15	11	36	0.64
At5g19140	AILP1	Plastid	Metal handling	1.05	0.05	7	8	0.66
At1g23290	RPL27A	Cytosol	Protein synthesis	0.97	0.05	5	5	0.72
At2g29630	THIC	Plastid	Cofactor and vitamin metabolism	0.89	0.09	10	28	0.78
At3g15840	PIFI	Plastid	Light reaction	0.87	0.10	8	8	0.80
At1g72930	TIR	Cytosol	Stress	0.84	0.14	7	11	0.82
At1g11910	APA1	Vacuole	Protein degradation	0.78	0.06	12	13	0.89
At3g20050	TCP-1	Cytosol	Protein folding	0.77	0.34	5	7	0.90
At5g19940	PAP	Plastid	Cell organization	0.76	0.03	9	9	0.91
At4g14030	SBP1	Cytosol	Metal handling	0.76	0.14	6	8	0.91
At1g22930	TCP-11	Nucleus	Not assigned	0.75	0.32	7	7	0.92
At3g02110	SCPL25	Extracellular	Protein degradation	0.73	0.02	9	9	0.94
At4g15545	NA	Nucleus	Not assigned	0.73	0.31	4	5	0.95
At1g42960	NA	Plastid	Not assigned	0.69	0.38	6	7	1.00
At5g62350	Invertase	Extracellular	Misc.	0.69	0.05	11	15	1.00

Protein accession number, short name, location in the cell, and functional category are shown for each protein. The protein's degradation rate (K_D) and its SE are shown along with the number of biological samples in which it was observed (Brep No.), the number of peptide spectra used to calculate the K_D, and the calculated half-life of the protein.

Lemberg, 2015). Neither grand average of hydrophobicity nor transmembrane domain number showed overall correlations with the K_D of proteins, but beta barrel structure proteins had very low K_D values compared with other groups of proteins (Supplemental Data Set 4C).

Many proteins do not operate as independent monomers in vivo but are present in strict stoichiometry in protein complexes. We tested the hypothesis that degradation rates of members of a complex would be more consistent with other members of the same complex than the wider set of cellular proteins. The members of seven major protein complexes representing the cytosol ribosome, proteasome, plastid ATP synthase, plastid ribosome, PSI, PSII, and mitochondrial electron transport chain were extracted from the 1228 data set, and all other proteins in the 1228 were considered in one group, designated as "Others." Outlier data for specific protein complexes and from the Others group were removed for the analysis. The SD (σ) was calculated for K_D values for each protein complex (Figure 4C, red line) with N subunits, and this was compared with 100,000 randomly sampled sets of the same N from the Others category (blue distributions). Probability values showed that in all cases, except the cytosolic ribosome, the standard deviations were significantly smaller for the complexes than for the random distribution sets of the same N. In a complementary approach, a pairwise Silhouette (Si) clustering comparison (Rousseeuw, 1987) was performed between each protein complex and Others. The ΔSi value (-2, 2) in each case showed the level of relative tightness of the K_D rates of the specific protein complexes compared with Others. Plastid ATP synthase, PSI, and proteasome had the highest ΔSi values and were thus the three protein complexes with the tightest distribution in terms of the degradation rates of their subunits (Supplemental Data Set 4D).

A protein's function or domain structure may also be a factor in defining its degradation rate. The high degradation rate of proteins has previously been explained based on specific features of a protein fold that enables rapid degradation in protein abundance, e.g., the auxin degron (Nishimura et al., 2009), or the irreversible binding of inhibitors to a protein domain or due to an enzymatic mechanism that damages an active site (e.g., self-hydrolyzing enzymes, reactive oxygen species damage, cosubstrate enzymes, or catalysis with suicide substrates) (Walsh, 1984; Chatterjee et al., 2011). To test systematically for domains in Arabidopsis proteins linked to degradation rate, we searched for differences in protein degradation rate distributions between protein sets with common protein domains. Fifty-eight nonredundant protein domain sets were selected for nonparametric k-sample K-W ($P < 0.01$) and C-I post-hoc testing (Table 2; Supplemental Data Set 4E). These protein domains can be divided into 10 groups (A–J) based on degradation rates. The four proteins containing the SH3 domain involved in translation were the most stable proteins (median of 0.05 d^{-1}), while the four proteins (three E2 and one E1 ligases) containing the ubiquitin-conjugating enzyme domain (median of 0.38 d^{-1}) were the most unstable.

Differences in Degradation Rate and Abundance of Specific Proteins in Leaves of Varying Ages

While overall protein degradation rates of individual proteins were relatively reproducible (median RSE of all peptide data or a protein ~10% and between leaf types in the rosette RSE ~16%; Supplemental Data Set 2B), there were specific proteins for which degradation rate appeared to be significantly influenced by the leaf from which the protein was derived. Analysis of these proteins

Downloaded from https://academic.oup.com/plcell/article/29/2/207/6099059 by guest on 20 August 2022

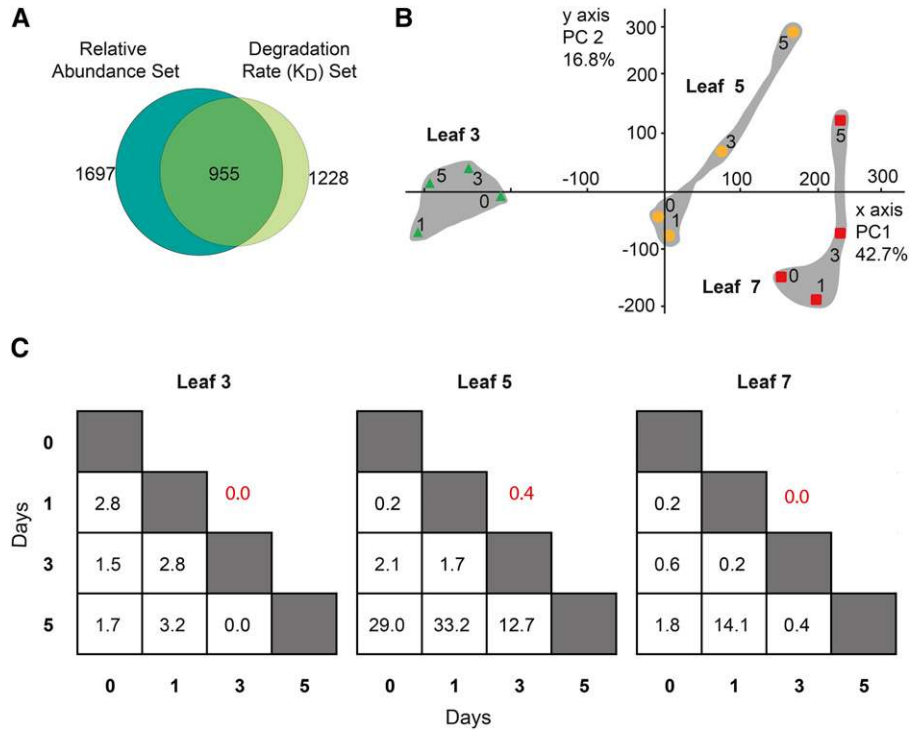

Figure 3. Changes in Relative Abundance Estimates for Individual Proteins in Leaves of the Arabidopsis Rosette during 5 d of Leaf Growth.

(A) The intersection of the number of specific proteins with a measured K_D value and a protein relative abundance assessment.
(B) Principal component analysis of specific protein abundances from MS analysis. Abundance data for 955 proteins (K_D values recorded in Figure 2) were used for the analysis. The clustering of leaf 3 (green), leaf 5 (yellow), and leaf 7 (green) is shown in the gray shading. The full data are provided in Supplemental Data Sets 3A and 3B.
(C) A matrix of paired statistical comparisons of protein abundance between day 0, day 1, day 3, and day 5 time points for each leaf is presented with the percentage of the proteins from **(B)** that significantly changed in abundance (*t* test $P < 0.01$) reported (full data in Supplemental Data Set 3C). Outside the matrix is the percentage of proteins measured that were found to change in abundance (*t* test $P < 0.01$) across the entire time course in each leaf.

allowed us to look for linkages between changes in protein degradation rate and protein relative abundance in two very different growth scenarios. Proteins in leaf 3 and leaf 7 were selected if they had significant differences in both protein abundance (Figure 5A, left; $P < 0.05$; 502 pairs) and degradation rate (right; $P < 0.05$; 433 pairs) and the set was separated into functional categories. Leaves 3 and 7 were chosen because proteins in their proteomes best reflected a steady state over time that could be described by a simple dilution effect (Figure 3). The abundance and degradation differences for these proteins were calculated as relative ΔAbundance and relative ΔK_D [i.e., (leaf 7-leaf 3)/average (leaf 3, 7)] and are each presented as box plots in Figure 5A. The dashed line indicates the point of parity between leaf 3 and leaf 7. Lower protein abundance in leaf 3 or 7 correlated with higher degradation rates for plastid proteins involved in cell organization, light reactions, stress, Calvin cycle, and photorespiration enzymes, while high protein abundances in leaf 3 or 7 correlated with low protein degradation rate for plastid proteins involved in tetrapyrrole synthesis, protein folding, and protein synthesis. When we focused on photosynthesis-associated proteins, and matched individual proteins across the data from leaves 3, 7, and 5, we found that there was a consistent correlation between relative abundance (Figure 5B) and protein degradation rate (Figure 5C) on a protein-by-protein basis across different protein complexes and metabolic pathways. In these experiments, leaf 5 K_D data sat neatly between that of leaf 3 and leaf 7, despite some concerns about the steady state assumption rising from Figure 3. A set of K_D values for 49 photosynthesis proteins were also independently calculated by regression analysis across all time points to ensure the effect was not due to the method of calculation. This alternative analysis gave effectively the same result, i.e., degradation rates were higher in leaf 7 than in leaf 3, with leaf 5 in between (Supplemental Figure 6 and Supplemental Data Set 5A). A set of 179 unique proteins with significant changes in both degradation rates and abundances between leaves 3 and 7 were then analyzed using correlation analysis. Nearly 85% of these proteins showed patterns of either increasing degradation rate and decreasing protein abundance, or decreasing degradation rate and higher protein abundance (Supplemental Data Set 5D).

Protein Kinetic Signatures of Leaf Growth

In hypertrophic mouse hearts, organ growth rate has been associated with disease, and differences in protein degradation rate have been used to propose the concept of "protein kinetic

Downloaded from https://academic.oup.com/plcell/article/29/2/207/6099059 by guest on 20 August 2022

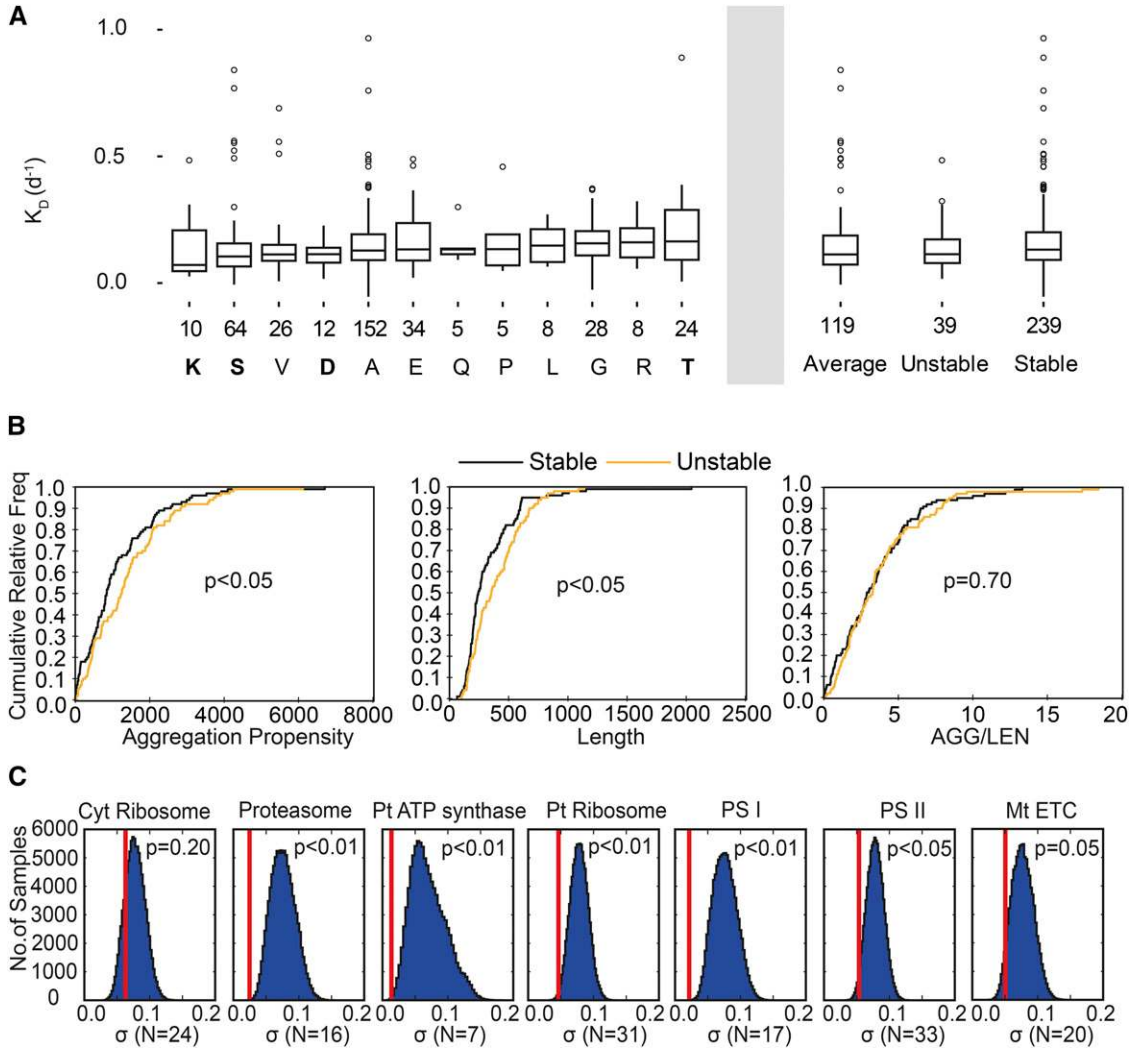

Figure 4. Intrinsic Properties of Arabidopsis Proteins That Correlate with Protein Degradation Rate.

(A) Comparison of protein degradation rate with the probable mature N-terminal amino acid residue (Supplemental Data Set 4A). Only protein sets in which more than five members had the same N-terminal amino acid residue were examined, a set of 376 proteins in total. A nonparametric Kruskal-Wallis k-samples test showed no significant difference among the 12 N-terminal groups. However, the K, S, and D groups showed significantly different degradation rate distributions from (T) by a Conover-Iman post-hoc test. No statistically significant differences were found when degradation rates of stable amino acids (A, V, M, G, T, and P), unstable amino acids (K, F, D, R, and Q), and average stability amino acids (all others amino acids) were compared (Supplemental Data Set 4A). These groups were defined based on the consensus of yeast and mammal N-end rules.

(B) A cumulative relative frequency distribution graph of protein aggregation propensity (AGG) of each protein, the amino acid length of each protein (LEN), and the ratio of AGG/amino acid length between the top 100 most stable and bottom 100 most unstable proteins from the set of 1228 proteins with degradation rates. Statistical significance was estimated by the Kolmogorov-Smirnov test.

(C) The SD (σ) of the protein degradation rates of the protein subunits of seven major protein complexes compared with randomly sampled distributions of σ for the same sized group of proteins from the set of 1228. The protein complexes were: cytosol ribosome, proteasome, Pt ATP synthase, Pt ribosome, PSI, PSII, and mitochondrial electron transport chain; all other proteins were considered to be one group "Others." The SD (σ) was calculated for each specific protein complexes with N subunits and then compared with the distribution of 100,000 random samplings of groups of size N from Others. The red line shows the σ value of a specific protein complex, while the blue distribution shows a histogram of σ values from the 100,000 random samplings of each value of N. The probability value is the proportion of 100,000 random samplings of N that show a smaller σ than the specific protein complex.

signatures" associated with cellular dysfunction (Lam et al., 2014). These kinetic signatures have been defined as proteins for which a change in degradation rate correlated with tissue growth rate. These rate-changing proteins were regarded as a new type of disease marker (Lam et al., 2014). We used the same principle here to determine if the degradation rate of specific leaf proteins could be correlated to leaf growth rate. In our case, these plant rate-changing proteins would be biomarkers associated with plant leaf growth rather than indicators of disease. By presenting protein degradation rates in different functional categories as a function of

Downloaded from https://academic.oup.com/plcell/article/29/2/207/6099059 by guest on 20 August 2022

Table 2. Average Degradation Rates of Groups of Proteins Containing the Same Protein Domain

Protein Domains	PD Code	No.	K_D (d^{-1}) Min.	K_D (d^{-1}) Max.	K_D (d^{-1}) Median	Group
Translation protein SH3-like domain	IPR008991	4	0.024	0.070	0.047	A
Glyceraldehyde-3-phosphate dehydrogenase, type I	IPR006424	4	0.051	0.076	0.069	A-B
Ribosomal protein L12 family	IPR027534	4	0.041	0.086	0.068	A-B
Bifunctional inhibitor/plant lipid transfer helical domain	IPR016140	4	0.054	0.093	0.064	A-B
PsbQ-like domain	IPR023222	4	0.050	0.095	0.070	A-B
NB-ARC	IPR002182	4	0.055	0.096	0.076	A-B
Zinc finger, PHD-type	IPR001965	4	0.060	0.093	0.080	A-B
Zinc finger, RING/FYVE/PHD-type	IPR013083	6	0.016	0.104	0.084	A-B
Serine/threonine-protein kinase, active site	IPR008271	4	0.025	0.104	0.080	A-B
Mitochondrial substrate/solute carrier	IPR018108	5	0.044	0.116	0.084	A-B
PsbP family	IPR002683	11	0.046	0.140	0.086	A-B
Chlorophyll a/b binding protein domain	IPR023329	14	0.040	0.173	0.079	A-C
Tetratricopeptide repeat	IPR019734	4	0.067	0.104	0.087	A-D
Protein kinase, ATP binding site	IPR017441	5	0.025	0.115	0.088	A-D
Transketolase-like, pyrimidine-binding domain	IPR005475	4	0.069	0.117	0.081	A-D
Riboflavin synthase-like β-barrel	IPR017938	4	0.064	0.137	0.080	A-D
Protein kinase-like domain	IPR011009	8	0.025	0.124	0.096	A-D
ATPase, α/β-subunit, nucleotide-binding domain	IPR000194	5	0.050	0.112	0.102	A-E
Galactose mutarotase-like domain	IPR011013	5	0.069	0.151	0.084	A-E
Aminoacyl-tRNA synthetase, class II (G/P/S/T)	IPR002314	6	0.068	0.135	0.093	B-E
Isocitrate/isopropylmalate dehydrogenase domain	IPR019818	4	0.037	0.135	0.107	B-E
Proteasome, subunit α/β	IPR001353	10	0.072	0.136	0.093	B-E
Glycoside hydrolase-type carbohydrate-binding, subgroup	IPR014718	4	0.084	0.151	0.091	B-E
Malate dehydrogenase, active site	IPR001252	5	0.025	0.181	0.123	B-E
Ribosomal protein S5 domain 2-type fold	IPR020568	8	0.034	0.178	0.103	B-E
HAD hydrolase, subfamily IA	IPR006439	4	0.069	0.152	0.101	B-F
Isopropylmalate dehydrogenase-like domain	IPR024084	5	0.037	0.135	0.115	B-F
Short-chain dehydrogenase/reductase, conserved site	IPR020904	4	0.058	0.148	0.116	B-G
PDZ domain	IPR001478	5	0.047	0.202	0.129	C-G
D-isomer-specific 2-hydroxyacid dehydrogenase domain	IPR029752	5	0.005	0.176	0.160	D-G
Aminotransferase, class I/class II	IPR004839	8	0.055	0.179	0.132	D-G
Threonyl/alanyl tRNA synthetase, SAD	IPR012947	4	0.097	0.168	0.119	D-H
Dehydrogenase, E1 component	IPR001017	4	0.071	0.204	0.128	D-H
Calycin	IPR012674	4	0.082	0.210	0.128	D-H
Fructose-bisphosphate aldolase, class I	IPR000741	6	0.093	0.224	0.114	D-H
Glutathione *S*-transferase, C-terminal	IPR004046	6	0.062	0.230	0.159	E-H
Clp, N-terminal	IPR004176	4	0.065	0.219	0.160	E-H
AMP-dependent synthetase/ligase	IPR000873	4	0.070	0.222	0.146	E-H
ATP-grasp fold, subdomain 1	IPR013815	7	0.063	0.271	0.160	E-H
14-3-3 protein, conserved site	IPR023409	7	0.096	0.185	0.129	E-H
Aldo/keto reductase	IPR001395	4	0.100	0.172	0.135	E-I
Thioredoxin domain	IPR013766	12	0.094	0.220	0.131	F-I
Immunoglobulin-like fold	IPR013783	5	0.103	0.171	0.152	F-I
Glutaredoxin	IPR002109	6	0.076	0.227	0.153	F-I
Pyridine nucleotide FAD/NAD(P)-binding domain	IPR023753	11	0.070	0.296	0.170	F-I
Thioredoxin	IPR005746	9	0.103	0.220	0.169	G-I
Alpha-D-phosphohexomutase superfamily	IPR005841	5	0.101	0.298	0.153	G-I
ATPase, AAA-type, conserved site	IPR003960	8	0.056	0.261	0.161	G-I
Tubulin/FtsZ, C-terminal	IPR008280	4	0.061	0.276	0.208	G-I
Alcohol dehydrogenase superfamily, zinc-type	IPR002085	8	0.097	0.266	0.164	G-I
Rossmann-like α/β/α sandwich fold	IPR014729	13	0.077	0.376	0.201	H-I
Immunoglobulin E-set	IPR014756	5	0.141	0.196	0.179	H-J
Ferredoxin [2Fe-2S], plant	IPR010241	4	0.130	0.267	0.194	H-J
Aconitase/3-isopropylmalate dehydratase domain	IPR001030	4	0.134	0.292	0.198	H-J
Pyruvate/phosphoenolpyruvate kinase-like domain	IPR015813	6	0.172	0.271	0.197	I-J
UspA	IPR006016	5	0.192	0.221	0.218	I-J

(Continued)

Downloaded from https://academic.oup.com/plcell/article/29/2/207/6099059 by guest on 20 August 2022

Table 2. (continued).

Protein Domains	PD Code	No.	K_D (d^{-1}) Min.	K_D (d^{-1}) Max.	K_D (d^{-1}) Median	Group
Peptidase, FtsH	IPR005936	4	0.162	0.261	0.238	I-J
Ubiquitin-conjugating enzyme/RWD-like	IPR016135	4	0.351	0.388	0.377	J

Shown are 58 protein domains (with at least four protein members per domain) that each had a tight average K_D distribution (median/SD > 2). Nonparametric k-sample K-W analysis ($P < 0.01$) and a C-I post-hoc test were used to divide the protein domains into groups A to J. Domains are listed by increasing degradation rates (all data in Supplemental Data Set 4E). The number of protein members (No.), K_D minimum, maximum, and median for each protein domain are shown.

the growth rates of leaves (Figures 6A to 6E; Supplemental Data Set 6A), we observed that the degradation rate of many photosynthesis-related proteins positively correlated with leaf growth rate, with the exception of chaperonin 60 proteins (Figure 6A). The latter have their highest abundance in the fastest growing leaf type, leaf number 7 (Figure 6F). For organelle ATP-dependent proteases, the degradation rate of FtSH class proteases positively correlated with growth, while the degradation rate of CLP, MAP, and DEG classes negatively correlated with growth rate (Figure 6C). Among the proteasome subunits and ubiquitination machinery, E3 ligases positively correlated with leaf growth rate, while the proteasome itself negatively correlated with leaf growth rate (Figure 6E). Among the subunits of the plastid and cytosolic ribosomes, there was a consistent negative correlation between protein degradation rate and leaf growth rate (Figures 6B and 6D).

But what could these correlations mean? A key biochemical impact of changing degradation rate as leaf growth rate changes is the alteration of the age profile of specific proteins in different leaves. For example, increasing the degradation rate of ribosomal proteins as leaves mature and slow their growth rate increases the proportion of new ribosomes in the mature leaf. Young growing leaves can achieve the same result by ribosome numbers increasing through growth, rather than replacement. As a result, both leaves maintain similar age profiles for ribosomes that are 0 to 8 d old (Supplemental Data Set 6B). By contrast, the slowing degradation rate of photosynthetic proteins as leaves slow their growth rate will mean distinctly older age profiles for these photosynthetic enzymes in mature leaf tissues. Our calculations of this effect show that ~90% of photosynthetic enzymes will be less than a week old in leaf 7 compared with only ~55% of photosynthetic enzymes in leaf 3 (Supplemental Data Set 6B).

Proportion of Energy Use in Degradation and Synthesis of Specific Protein Classes in Different Leaves

We also estimated total ATP costs from protein degradation and synthesis in the three leaf types from the Arabidopsis rosette by summing up the costs for all the 1228 proteins in our data set. This used protein degradation rates, calculated protein synthesis rates, leaf growth rate, and the steady state of the leaf proteome and coupled them with individual protein lengths. We used a 5.25 ATP per amino acid residue cost of synthesis (including amino acid synthesis, ribosome translation, and transport) and 1.25 ATP per amino acid residue cost of degradation (unfolding) and estimated relative protein abundance based on modified estimates from PaxDb (see Methods for details of calculations and references; see Supplemental Data Set 7A for details). The set of 1228 proteins we measured account for the bulk of protein abundance in Arabidopsis leaves (nearly 90% of all Arabidopsis leaf protein based on ppm counts from PaxDb and RBCL measurement). Assuming that cellular respiration is the primary net ATP production source in leaves, the relative proportion of ATP used for protein synthesis and degradation could also be determined using leaf respiration rates of the Arabidopsis rosette (Sew et al., 2013). In leaves that are not growing (e.g., leaf 3 in this study), synthesis of new protein is simply replacing degraded protein and would cost 13% of cellular ATP. By contrast, in leaf 7, which was rapidly growing, synthesis costs reached 38% of total respiratory ATP (Figure 7A). This analysis also showed that the overall ATP cost of protein degradation was ~4% of respiratory ATP synthesis across all leaf types. When the protein abundance of plastids and relatively high number of higher turnover proteins in the plastid were considered, nearly 70% of synthesis and degradation costs were attributable to the plastid, with the cytosolic proteome representing 10% of costs and other organelles all having relatively small percentage costs (Figure 7B; Supplemental Data Set 7B). Within functional categories, the Calvin cycle and light reactions alone represented nearly 50% of all protein synthesis and degradation costs. We also used these data to highlight the set of proteins in Arabidopsis that each account for more than 1% of total protein turnover costs in leaves (Figures 7C and 7D, Table 3; Supplemental Data Set 7C). The subunits of Rubisco represented 13 to 18% of all protein costs, while representing ~17% of total cell protein abundance. Some proteins were on this list largely owing to their rapid degradation rate rather than their large abundance; for example, the PSII D1 subunit was expected to be a high cost protein, while AOS and THI1 have not typically been considered as large energy costs to the plant cell but each represented more than 1% of total ATP costs for protein turnover (Figures 7C and 7D).

DISCUSSION

Key Considerations in Assessing Plant Protein Degradation Rates in Growing Leaves

Calculations of protein degradation require information on whether the proteome is in steady state and how increases in protein abundance relate to organ or tissue growth rate. Most historical studies in mammals have assumed steady state to be the case in short time frames where no treatments were imposed (Price et al., 2010; Cambridge et al., 2011; Schwanhäusser et al., 2011). In plants, some reports have attempted to measure changes in protein abundance of specific targets of interest

Downloaded from https://academic.oup.com/plcell/article/29/2/207/6099059 by guest on 20 August 2022

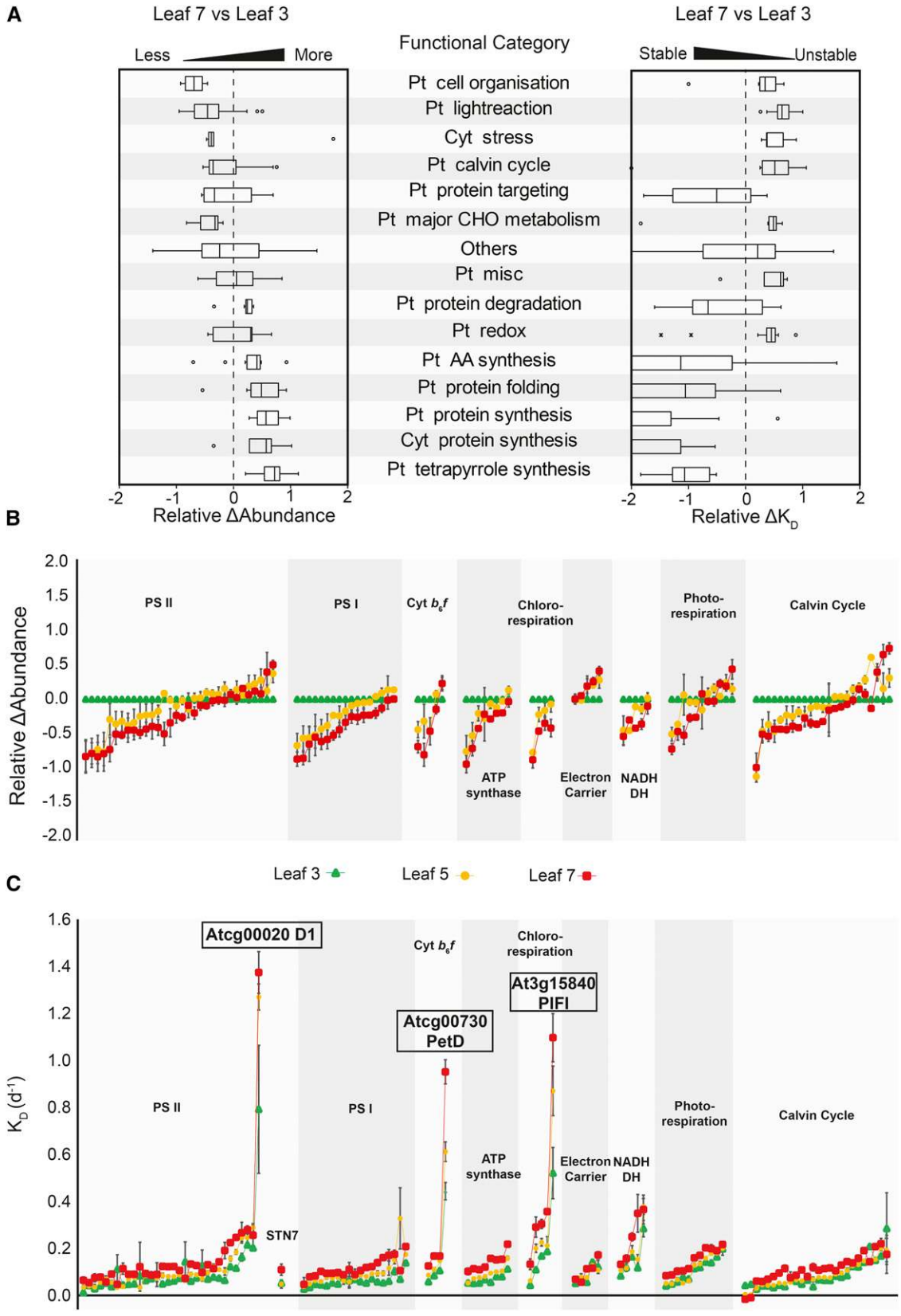

Figure 5. Comparisons of the Relative Protein Abundance and Degradation Rate of Specific Proteins That Differed in Their Measurements between Leaf 3 and Leaf 7.

(A) Proteins with significant changes (*t* test, $P < 0.05$) in abundance (502 pairs, left) or degradation rate (433 pairs, right) between leaf 3 and leaf 7 are presented. The changes in relative abundance and degradation rate are shown as relative ΔAbundance and ΔK_D by comparing leaf 7 to leaf 3 data. Major

Downloaded from https://academic.oup.com/plcell/article/29/2/207/6099059 by guest on 20 August 2022

(Li et al., 2012; Lyon et al., 2016), and others have relied on linear regression across a time series to remove outliers and thus only retain information when turnover rates have not changed (Yang et al., 2010; Nelson et al., 2014; Fan et al., 2016). However, these approaches have their limitations in plants and are prone to both error and to the removal of interesting biological features of interest in the data. Notably, regression analysis focuses on the increasing abundance of newly synthesized protein that is mainly derived from growth in plant systems and masks the real kinetics of the protein degradation process. In addition, plant protein turnover studies have typically provided a list of protein degradation rates, without any comparative evaluation of changes in degradation during growth and development. To address these issues, we have taken a series of approaches. First, we undertook a quantitative proteomics analysis within and between different leaves within the Arabidopsis rosette after the 10th leaf had appeared and followed changes in these leaf proteomes over the 5 d required for a ^{15}N labeling strategy to yield a substantial list of protein degradation rates. This has shown that in leaves 3 and 7, the relative abundance of 97 to 99% of relatively high abundance proteins within each leaf type did not significantly change on a per unit protein basis, even though total protein per leaf increased at different rates over 5 d. The apparent steady state evident in leaves 3 and 7 was less valid in leaf 5, in which only 80 to 90% of the proteome remained unchanged in relative abundance over the 5 d of labeling. This illustrates that while quasi-steady states of proteomes can be found during plant leaf growth, these need to be experimentally measured and confirmed before an analysis strategy is implemented that relies of this principle. That said, we observed that the changes that were measured in leaf 5 were not consistent across all time points and the scale of the fold changes did not typically alter the nesting of K_D values from leaf 5 in analysis of data sets (e.g., Figures 5 and 6). Second, we used paired data at different time points to calculate average protein degradation rates rather than linear regression across all time points. This enabled more fast and slow degradation rates to be measured and variable rates to be averaged across time points and peptides, rather than these data being discarded (Li et al., 2012). Third, we observed that protein abundance per gram fresh weight (FW) varies in Arabidopsis leaves during development (Supplemental Figure 1); hence, it was important to focus our calculations of dilution of ^{14}N-labeled peptides on the increase in leaf protein content rather than on size or weight of each leaf. This observation is consistent with independent evidence that young leaf total protein content changes over time in Arabidopsis as a proportion of leaf size (Ishihara et al., 2015).

Protein Features Linked to Degradation Rate

The >150-fold variation of protein degradation rates of the ~1000 relatively abundant proteins in Arabidopsis leaves raises significant questions about which protein characteristics define the degradation kinetics of different protein types. The availability of these degradation rates provided an opportunity to explore a range of possible hypotheses and provide some statistical comparisons of degradation rates for different groups of proteins. It is well established that the proteolysis machinery of the cell is spatially distributed and the latency of proteins in different cellular locations varies, which means that not all proteins will be acted upon by the same protease network or in the same timeframe (van Wijk, 2015). Using subcellular location information as a basis for dissecting the data set, we observed lower protein degradation rates in metabolic organelles that are separated from the cytosol by phospholipid membranes and higher protein degradation rates in the endomembrane system, which is directly involved in protein synthesis and traffics proteins to the plasma membrane. This suggests that there are broad spatially based groupings in the proteome that set a median rate of degradation of proteins in different subcellular compartments. However, quantitatively these patterns represent <2-fold of the variation in median degradation rates. Diurnal fluctuation in transcription could be a marker for a heightened turnover rate for specific proteins in the light or the dark. Our analysis of this effect failed to see a significant correlation in the data as a whole, but we did observe that proteins with light-induced transcriptional patterns were enriched in the set of proteins with faster K_D. This indicates that light-dependent transcriptional processes may be associated with enhanced protein degradation of the proteins being synthesized, while dark-dependent processes are relatively less connected.

Although the N-terminal residue of a polypeptide has some reported influence on turnover rate for subsets of plant proteins (Apel et al., 2010; Zhang et al., 2015), the N-terminal residue alone appeared to have little predictive value in our data set to define the turnover rate of unknown sets of protein of different sequences (Figure 4A). Protein aggregation propensity has been linked to protein degradation rate and has been shown in other eukaryotic systems to be independent of protein size (De Baets et al., 2011). In our Arabidopsis data set, aggregation propensity and protein size

Figure 5. (continued).

functional categories (as in Figure 2) that comprised at least five proteins for abundance or degradation data are displayed. All remaining proteins were combined in the Others group. Outliers are presented as hollow dots. The dashed line shows the boundary for no change in abundance and degradation between leaf 3 and leaf 7.

(B) Relative ΔAbundance was compared for leaves 3, 5, and 7 for photosynthesis protein complexes and functional categories (110 proteins). The proteins on the *x* axis are in the same order for each leaf comparison. Error bars show standard errors of relative ΔAbundance from each leaf separately; all comparisons are relative to leaf 3.

(C) Protein degradation rates (K_D) was compared for leaves 3, 5, and 7 for photosynthesis protein complexes and functional categories (116 proteins). The proteins on the *x* axis are in the same order for each leaf comparison. Average K_D and standard errors calculated from data for each leaf separately are shown. The proteins in **(B)** and **(C)** are not in the same order but are shown in rank order within each complex to show the consistent trend in relative ΔAbundance and protein degradation rates (K_D) across the three leaves.

Downloaded from https://academic.oup.com/plcell/article/29/2/207/6099059 by guest on 20 August 2022

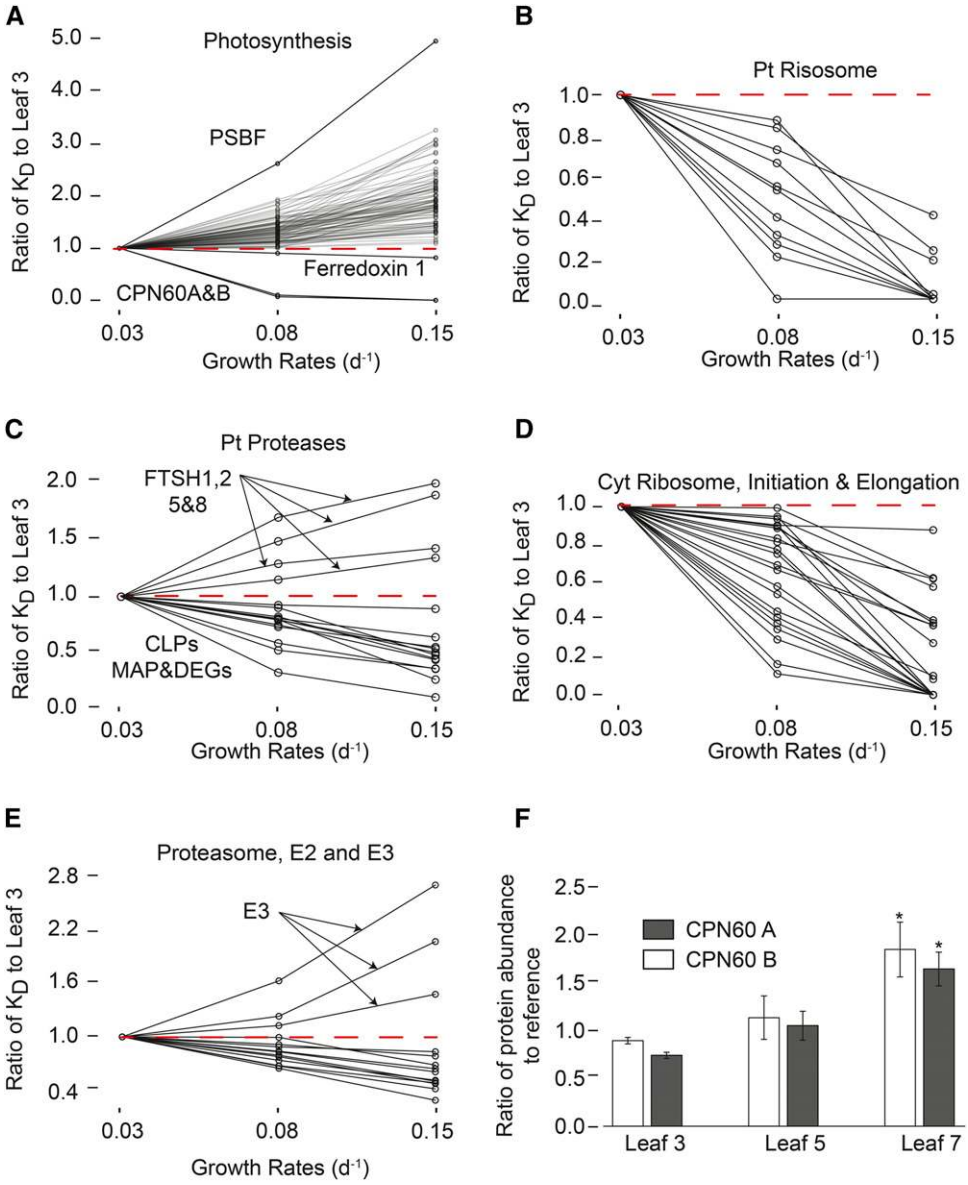

Figure 6. Correlation of Arabidopsis Protein Degradation Rates with Leaf Growth Rate.

(A) to **(E)** Protein degradation rates (K_D) in leaves 5 and 7 were normalized to corresponding values for the same proteins in leaf 3. Ratios of K_D to leaf 3 K_D values for 92 photosynthesis proteins **(A)**; 11 plastid ribosome proteins **(B)**; plastid proteases including CLPs (CLPP2, CLPP5, CLPP6, CLPC, CLPR1, CLPR2, CLPR4, CLPR6, and Clp), DEG (DEGP1 and DEGP2), MAP, and FTSHs (FTSH1, FTSH2, FTSH5, and FTSH8) **(C)**; 12 cytosol ribosome proteins and 10 initiation and elongation proteins **(D)**; and proteasome E2 and E3 ligase proteins **(E)** are shown plotted against the leaf growth rates of leaves 3, 5, and 7. All proteins shown had positive or negative Pearson correlations between the ratio of K_D and leaf growth rate of $R > 0.9$ or $R < -0.9$, respectively. The red dashed line is a boundary for negative and positive correlations.

(F) The relative protein abundance of CPN60 A and B in leaves 5 and 7 is compared with leaf 3 (*$P < 0.05$). Error bars are SE of all data from each leaf separately.

both correlated with turnover rate when the extremes of the fast and slow degradation distribution were compared, but when the higher aggregation propensity of large proteins was accounted for, there was no longer a relationship with degradation rate (Figure 4B). This suggests that while aggregation propensity could account for some differences in degradation rate, as shown in mammals, it is mainly due to protein length rather than amino acid composition of proteins in Arabidopsis. Subunits of protein complexes might be expected to turn over at similar rates, and this was largely confirmed when six out of seven physical complexes or protein systems were found to show significantly tighter distributions of degradation rates compared with random samplings of proteins (Figure 4C). This means that comembership of a complex could be a useful predictive tool for predicting unknown

Downloaded from https://academic.oup.com/plcell/article/29/2/207/6099059 by guest on 20 August 2022

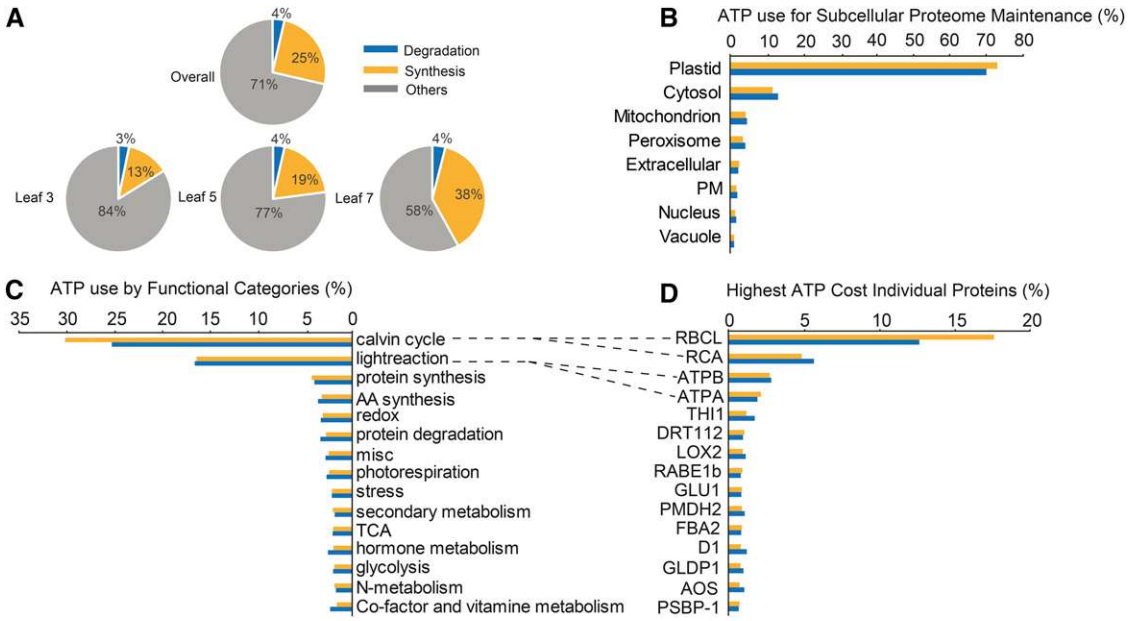

Figure 7. ATP Energy Budgets for Protein Degradation and Synthesis in Arabidopsis Leaves.

(A) The proportion of cellular ATP used for protein degradation (blue), protein synthesis (yellow), and other aspects of cell maintenance (gray). Energy budgets are presented as the averages across leaves 3, 5, and 7 and in each leaf individually.
(B) The proportion of ATP used for protein degradation (blue) and synthesis (yellow) in maintaining the proteomes of major cellular organelles and structures (when ATP cost >1% of total ATP use).
(C) ATP used for protein degradation (blue) and synthesis (yellow) by major functional categories of proteins (when ATP cost >2% of total ATP use).
(D) The 15 individual proteins with the highest ATP cost to maintain in the Arabidopsis proteome; only four of these were from the two highest cost functional categories (dotted lines). Subcellular location, functional categories, and specific high cost proteins were sorted by the proportion of energy cost for protein synthesis (yellow). Respiration was presumed to be the primary net ATP production source for protein synthesis, and its value is based on experimental data from the Arabidopsis rosette.

protein degradation rates. Specific protein fold families and domain groups were shown by this analysis as the major factors that could be used to predict degradation rates (Table 2). Nearly 40-fold differences in degradation rate were observed for proteins in different domain classes.

Protein Stability and the Correlations with Protein Function

One essential goal of protein degradation studies is to help elucidate the biological functions of specific proteins based on their variable turnover rates, and to this end efforts have been made in correlation analysis of protein turnover and protein biological functions across different organisms (Schwanhäusser et al., 2011; Christiano et al., 2014; Karunadharma et al., 2015). Consistent with evidence in yeast (Christiano et al., 2014), ribosomal subunits are some of the most stable and long-lived proteins in Arabidopsis (Figure 2A). This means ribosomal proteins can be used for a long time period after their biogenesis, with their abundance controlled posttranslationally by protein degradation at late stages of development. However, even in these long-lasting protein sets, the relative degradation rate distribution for the cytosolic ribosome had a higher SD than those of other protein complexes (Figure 4C). These nonuniform degradation rates in the cytosolic ribosome may be related to the specialized role of structural subunits in ribosome and altered stages of assembly, which has been proposed in a ribosome turnover study in human cells (Doherty et al., 2009).

Within photosynthetic complexes (Figure 5C), it was evident that three proteins had high degradation rates, well beyond the normal distribution for their complexes. While D1 (Atcg00020) is well known for its high degradation rate at the reaction center of PSII (Melis, 1999; Takahashi and Badger, 2011; Lambreva et al., 2014), the discovery that PetD (Atcg00730) of the cytochrome b_6f complex and PIFI (At3g15840) of the NDH complex had comparable degradation rates was not anticipated. These three proteins are core components required for electron transport functions of PSII, cytochrome b_6f, and NDH complexes. Interestingly, PetD is subject to proteolysis in highly purified cytochrome b_6f complex in vitro even in the presence of protease inhibitors, by an unknown mechanism (Zhang and Cramer, 2004). PIFI has been shown to be essential for NDH complex-mediated chlororespiration in Arabidopsis and PIFI knockout mutants exhibit a greater sensitivity to photoinhibition (Wang and Portis, 2007). Their fast degradation rate in vivo might reveal some functional similarity of these proteins in their respective protein complexes. D1 and PetD proteins are both chloroplast encoded. D1 is at the plastoquinone binding site of PSII and is directly involved in coordinating and protecting the metal cluster responsible for producing oxygen and protons from water (Umena

Downloaded from https://academic.oup.com/plcell/article/29/2/207/6099059 by guest on 20 August 2022

Table 3. ATP Cost of Protein Degradation and Synthesis for Major Functional Categories of Leaf Proteins

Functional Categories	No.	K_D (d^{-1}) Mean	K_D (d^{-1}) SD	Deg. Cost (%)	Syn. Cost (%)
Photosynthesis (48.9%)					
Calvin cycle	27	0.11	0.09	25.2	30.1
Light reaction	84	0.13	0.15	16.5	16.3
Photorespiration	11	0.12	0.05	2.7	2.4
Metabolism (18.4%)					
Amino acid synthesis	50	0.19	0.22	3.6	3.2
Secondary metabolism	33	0.18	0.13	1.8	2.0
TCA	31	0.12	0.05	2.1	2.0
Hormone metabolism	15	0.25	0.18	2.5	2.0
Glycolysis	24	0.14	0.05	2.0	1.9
Cofactor and vitamin metabolism	10	0.38	0.60	2.3	1.6
Major CHO metabolism	17	0.25	0.36	1.3	1.1
Lipid metabolism	29	0.13	0.09	1.1	1.1
Tetrapyrrole synthesis	16	0.12	0.07	1.1	1.0
Nucleotide metabolism	26	0.13	0.11	1.0	1.0
C1 metabolism	12	0.14	0.04	1.1	0.9
ETC	21	0.12	0.08	0.3	0.3
Minor CHO metabolism	10	0.15	0.07	0.2	0.2
Protein (8.9%)					
Protein synthesis	76	0.08	0.14	4.0	4.2
Protein degradation	81	0.17	0.14	3.3	2.8
Protein folding	24	0.12	0.17	0.7	0.8
Protein targeting	18	0.13	0.08	0.5	0.5
Protein amino acid activation	20	0.15	0.12	0.5	0.4
Protein PTMs	16	0.15	0.08	0.2	0.2
Stress and signaling (8.3%)					
Redox	52	0.15	0.08	3.3	3.1
Misc.	53	0.16	0.11	2.8	2.5
Stress	43	0.19	0.30	2.1	2.1
Signaling	26	0.14	0.08	0.7	0.6
Cell (2.6%)					
Cell organization	22	0.19	0.16	1.5	1.3
Cell cycle	14	0.14	0.10	0.9	1.0
Cell wall	20	0.17	0.10	0.4	0.3
RNA and DNA (2.2%)					
RNA binding	13	0.15	0.10	1.3	1.2
RNA regulation	33	0.12	0.07	1.0	1.0
DNA	11	0.13	0.10	0.1	0.1
Transport and metal handling (1.6%)					
Transport	31	0.12	0.06	1.4	1.3
Metal handling	11	0.33	0.31	0.5	0.3
Other (9.1%)	248	0.15	0.12	9.7	9.1

Major functional categories were divided into seven groups. Minor functional categories and nonassigned proteins were grouped together as "Other." Functional categories were sorted by the proportional cost of protein synthesis. The number of proteins in each group, K_D mean, and SD are shown.

et al., 2011; Lambreva et al., 2014; Wei et al., 2016).Cyanobacterial PetD forms the p-side of the cytochrome b_6f complex, which accepts protons from plastosemiquinone and defines a route for H^+ transfer in the complex (Hasan et al., 2013). Also, the transcripts for D1 and PetD proteins are both found to be upregulated in the *adg1-1 tpt-2* double mutant, which shows rapid photoinhibition under high light (Schmitz et al., 2014). D1 protein is widely recognized as a major target in PSII in the photodamage and photoprotection cycle (Melis, 1999; Takahashi and Badger, 2011). PetD and PIFI, like the D1 subunit, might represent new targets for light or other active electron and proton transfer pathway-associated damage and repair processes.

Protein Abundance and Turnover Changes in Young Leaves with Rapid Chloroplast Division

We observed that plastid-localized light reaction and Calvin cycle proteins showed lower protein abundance coupled with lower protein stability in leaf 7 (Figure 5), while ribosomal proteins showed higher stability and accumulated in the fast-growing leaf 7 (Figure 5A). This supports the proposal that regulatory mechanisms for accumulation of ribosomal proteins in fast-growing stages in plants is independent of transcript abundance but more likely due to stabilization of the assembled ribosome complexes (Baerenfaller et al., 2012; Ponnala et al., 2014). Increased levels of

Downloaded from https://academic.oup.com/plcell/article/29/2/207/6099059 by guest on 20 August 2022

synthesis, folding, and degradation proteins could provide high protein synthesis and degradation capability in younger leaves. This may in turn explain faster turnover of a range of metabolic protein sets in younger leaves, such as Calvin cycle and photorespiratory enzymes and light reaction complex subunits (Figures 5A and 5C).

Analysis of the relative protein degradation changes with leaf growth rate (Figure 6) highlighted that while the degradation rate for the majority of the photosynthetic apparatus components positively correlated with growth (Figure 6A), those of CPN60A and CPN60B negatively correlated with growth. These chaperonins are needed for plastid division (Suzuki et al., 2009), so their increased stabilization and abundance (Figure 6F) are consistent with the more frequent chloroplast division events that occur in young leaves (Osteryoung and Pyke, 2014). The selective degradation changes observed in younger leaves could also be caused by specific changes in proteolysis and translational control when leaves are growing at a faster rate. Analysis of relative protein degradation rates versus leaf growth rate (Figure 6) highlighted that while turnover of protein synthesis components negatively correlated with growth (Figures 6B and 6D), there were specific classes of organelle proteases whose turnover rate positively correlated with growth. The FtsH protein set highlighted in Figure 6 are the same proteins that are highlighted in the protein domain set FtsH (IPR016135), which was one of the fastest degrading domain groups in our analysis (Table 2). These proteases have direct roles in the turnover of the photosynthetic apparatus and in plastid thylakoid formation (Zaltsman et al., 2005; Kato et al., 2012; Rowland et al., 2015). It has been reported that mRNA for FtsH1, FtsH2, FtsH5, and FtsH8 generally increases in young developing leaves (Zaltsman et al., 2005). High mRNA levels for these proteases provides a fast synthesis potential, which is consistent with our finding that FtsH1, FtsH2, FtsH5, and FtsH8 exhibit rapid rates of degradation in younger leaves mostly without large changes in relative abundance (Figure 6C; Supplemental Data Set 8).

However, plastid turnover is controlled not only by internal proteases but also by the proteasome and vacuolar quality control pathways mediated by E3 (Ling et al., 2012; Woodson et al., 2015). Ubiquitination plays a role in control of plastids via a RING-type ubiquitin E3 ligase, SP1, which mediates the ubiquitination and degradation of TOC components that are required for developmental transition of plastids (Ling et al., 2012; Huang et al., 2013). Most recently, the plant U-box E3 ligase PUB4 was found to mediate the ubiquitination and selective degradation of damaged chloroplast through globular vacuoles (Woodson et al., 2015). While the proteasome subunit degradation rate was low in young leaves, the degradation rates of three E3 ligases we identified (one RING-type At1g57800 and two F-box At4g39756 and At5g01720) were higher in younger leaves (Figure 6E). Enhanced degradation of selective E3 ligases in younger leaves could thus also help maintain fast chloroplast biogenesis in younger leaves. However, it is still unclear whether this is achieved by promotion of developmental transition and/or by selective breakdown of damaged plastids.

Energy Costs of Leaf Protein Turnover

It has been widely accepted that active transport and protein turnover are the two highest cost processes in cell biology (Scheurwater et al., 2000). Calculations of energy costs for protein turnover depend on knowing the synthesis and degradation rates of proteins, as well as the length and abundance of each protein. This study provided the rate data, length is straightforward to determine, and abundance was estimated used the PaxDb estimates for Arabidopsis leaves (pax-db.org/). Expressing this ATP demand for protein synthesis and degradation as a proportion of available cellular ATP requires a cellular ATP synthesis rate calculation. While mitochondria are the primary ATP source in all eukaryotes, chloroplasts can also produce ATP through photophosphorylation in plants. Early studies showed that isolated intact chloroplast protein synthesis could be driven by light or added ATP, while etioplast protein synthesis could be driven only by added ATP (Siddell and Ellis, 1975; Ellis, 1981). This demonstrated that photophosphorylation and ATP imported through transporters could both be energy sources for chloroplast protein synthesis. However, several more recent calculations concluded that in planta additional ATP needs to be imported into chloroplast through translocators to meet the demands of CO_2 assimilation and photorespiration without even considering the energy cost of other biosynthetic processes including protein synthesis (Flügge et al., 2011; Kramer and Evans, 2011). This leaves chloroplasts dependent on import of respiration-derived ATP for most biosynthetic processes including protein synthesis. The importance of ATP import for chloroplast maintenance is also evident by reports that restriction of ATP import through NTT translocators can lead to dwarf and necrotic leaf phenotypes (Reinhold et al., 2007) and can disrupt hormonal signaling (Schmitz et al., 2010). Our calculations are based on the caveat that respiration is the only net source of ATP available for protein synthesis in plants. The dominance of the plastid proteome as a major energy cost through these calculations supports the importance of ATP import into chloroplasts based on the insufficiency of ATP supply from photophosphorylation.

Our data show that on a leaf basis the degradation costs were effectively static at ~4%, while synthesis rates varied considerably with the rate of leaf growth. Protein synthesis and degradation together cost ~16% of the total leaf oxidative phosphorylation-dependent ATP production in developed leaves with slow growth rates and ~42% in developing leaves with fast growth rates. This analysis suggests the protein turnover energy budget is one of the highest maintenance costs in growing Arabidopsis leaves. The Calvin cycle and the protein machinery of the light reactions are the highest cost functions in the growing Arabidopsis leaf (Figure 7, Table 3). These categories also share the top five high energy cost individual proteins. Interestingly, photorespiration proteins in plastids, mitochondria, and peroxisomes are all among the top 20 proteins in terms of energy cost (Supplemental Data Set 7A). Changes in the degradation rates or abundance of high energy cost proteins could cause significant fluctuations of the total energy budget and alter the ability of cells to reach a new balance between energy supply and consumption. The availability of a direct calculation of energy cost for specific proteins under different growth rates in an individual leaf will help to explain energy constraints in changing the abundance of specific proteins.

Downloaded from https://academic.oup.com/plcell/article/29/2/207/6099059 by guest on 20 August 2022

METHODS

Hydroponic Growth of Arabidopsis

Arabidopsis thaliana accession Columbia-0 plants were grown under 16/8-h light/dark conditions with cool white T8 tubular fluorescent lamps 4000K 3350 lm (Osram) with intensity of 100 to 125 μmol m^{-2} s^{-1} at 22°C. The hydroponic protocol was as described previously (Waters et al., 2012) and used a modified Hoagland solution (2 mM $CaCl_2$, 6 mM KNO_3, 0.5 mM NH_4NO_3, 0.5 mM $MgSO_4$, 0.25 mM KH_2PO_4, 0.05 mM KCl, and 0.04 mM Fe-EDTA) supplemented with micro elements [25 μM H_3BO_3, 2 μM $MnCl_2$, 2 μM $ZnSO_4$, 0.5 μM $CuSO_4$, 0.15 μM $CoCl_2$, and 0.25 μM $(NH_4)_6Mo_7O_{24}$] and 2.6 mM MES, and the pH was adjusted to 5.8 to 6.0. Seeds were planted on the surface of stone wool stuffed in 1.5-mL black tubes with the bottoms cut out to sit in 24-well floater tubes racks containing 160 mL growth medium. The seeds were vernalized under 4°C for 2 to 3 d before being transferred to the growth chambers. Half-strength growth medium was used for the first week. A single plant was placed in every tube and four tubes in each floater tube rack (Supplemental Figure 1A). The growth medium was changed every 7 d.

Unlabeled Arabidopsis plants were grown for 21 d until they reached leaf production stage 1.10 (T0) (Boyes et al., 2001) in natural abundance medium as noted above. Leaves 3, 5, and 7 from three biological replicates were collected at T0 (21 d), T1 (22 d), T3 (24 d), and T5 (26 d). Thirty-six unlabeled leaf whole protein samples were extracted and protein concentration from each leaf was determined by an amido black assay.

For progressive ^{15}N labeling, plants were also grown for 21 d until they reached leaf production stage 1.10 (T0) (Boyes et al., 2001) in natural abundance medium. The growth medium was then discarded and the growth racks rinsed four times with fresh medium without nitrogen (no KNO_3 or NH_4NO_3) to ensure the old solution was washed out. A total of 160 mL of ^{15}N medium (6 mM $K^{15}NO_3$ and 0.5 mM $^{15}NH_4^{15}NO_3$) was added for every four plants and the plants were grown for 1, 3, and 5 d (T1, 3, and 5) before collecting leaf numbers 3, 5, and 7 for total protein extraction (Supplemental Figure 1A). Four leaves numbered 3, 5, or 7 from plants in one rack were pooled as a biological replicate. Three biological replicates were collected at each time point. Twenty-seven ^{15}N labeled (T1, 3, and 5) and nine unlabeled samples (T0) were collected and stored separately for later analysis.

To obtain a fully labeled ^{15}N protein reference standard, ^{15}N medium (with 6 mM $K^{15}NO_3$ and 0.5 mM $^{15}NH_4^{15}NO_3$) was used to replace the natural abundance nitrogen in the medium and plants were grown from seed in this medium for 26 d (T5). ^{15}N labeling efficiency in leaf numbers 3, 5, and 7 was analyzed separately and each showed 98% ^{15}N incorporation (determined from median of 1500–2000 peptides). Fully ^{15}N labeled total proteins from leaf 3, 5, and 7 samples were pooled and used as ^{15}N fully labeled proteins reference for subsequent experiments.

FCP Following Leaf Production Stage 1.10

Aliquots of the 36 unlabeled leaf samples (T0, 1, 3, and 5) noted above were also used for FW and protein content measurements (Supplemental Figure 1). Liquid nitrogen snap frozen samples (0.1 g) were vortexed with Qiagen tissue lysis beads (5 mm) and boiled in 1× sample buffer (2% [w/v] SDS, 62.5 mM Tris-HCl, 10% [v/v] glycerol, 5% [v/v] mercaptoethanol, and 0.005% bromophenol blue) for 5 min and then centrifuged at 10,000*g* for 10 min. The supernatant was collected and separated with SDS-PAGE on Bio-Rad Criterion precast gels (10–20% [w/v] acrylamide, Tris-HCl, 1 mm, 18-well comb gels). Electrophoresis was performed at 300 V for 15 to 20 min. Proteins were visualized by colloidal Coomassie Brilliant Blue G 250 staining. ImageJ was used to quantify protein content in each sample (Supplemental Figure 1B). FCP was determined by combining fresh weight and protein content changes (Supplemental Data Set 1).

Determining Changes in Specific Protein Abundance over 5 d Using a Fully Labeled ^{15}N Protein Reference Standard

A total of 50 μg of each the 36 unlabeled leaf protein samples noted above was mixed individually with 50 μg of the fully ^{15}N-labeled reference and digested in solution by trypsin. Each sample was separated into 96 fractions by high pH HPLC separation and further pooled into 12 fractions. A total of 432 fractions from 36 samples were analyzed by mass spectrometry. Filtered samples (5 μL each) were loaded onto a C18 high-capacity nano LC chip (Agilent Technologies) using a 1200 series capillary pump (Agilent Technologies) as described previously. Following loading, samples were eluted from the C18 column directly into a 6550 series quadrupole time-of-flight mass spectrometer (Agilent Technologies) with a 1200 series nano pump using the following buffer B (0.1% formic acid in acetonitrile) gradient: 5 to 35% in 35 min, 35 to 95% in 2 min, and 95 to 5% in 1 min. Parameter settings in the mass spectrometer were as described previously (Nelson et al., 2014).

Agilent .d files were processed by an in-house script written in Mathematica for partial ^{15}N labeling quantification (Nelson et al., 2014) modified to calculate the ratio between ^{14}N peptide (L) and fully ^{15}N-labeled reference peptide (H). L and H formed two separate populations by a non-negative least square approach as described previously (Guan et al., 2011; Nelson et al., 2014). All filters used for partial ^{15}N labeling were kept (Nelson et al., 2014) and two more filters were applied: First, a minimum 80% ^{15}N enrichment was required to disregard quantifications with high noise level between L and H; second, a minimum signal-to-noise ratio of 5 was used to disregard high neighboring noise contribution to L and H. A total of 432 Agilent .d files were further processed by Trans Proteomic Pipeline to get protein probabilities for identification. Only proteins with $P > 0.95$ (false discovery rate [FDR] < 0.6%) were further reported. Examples for CPN60A (At2g28000), HPT108 (At3g63190), and PGK1 (PHOSPHOGLYCERATE KINASE1; At3g12780) in leaves 3, 5, and 7 are shown in Supplemental Figure 7.

Protein abundance was represented as ratio to reference. Protein abundance comparison of the same protein from leaves 3 and 7 was presented as relative ΔAbundance [i.e., (leaf 7 abundance–leaf 3 abundance)/average (leaf 3 and leaf 7 abundance)]. The processed quantification data are provided in Supplemental Data Set 9, and the peptide identification data for each time point are provided in Supplemental Data Sets 10 to 13.

Protein Separation, Digestion, MS Analysis, and Determination of Peptide ^{15}N Incorporation Ratio

The 27 ^{15}N progressively labeled and three unlabeled leaf samples (0.1–0.2 g) were snap frozen in liquid nitrogen and homogenized using Qiagen tissue lysis beads (5 mm) by vortex. A total plant protein extraction kit (PE0230-1KT; Sigma Chemicals) was used to extract total proteins. The final pellet of total protein was dissolved in solution 4 and then reduced and alkylated by tributylphosphine and iodoacetamide as described in the Sigma manual. The suspension was centrifuged at 16,000*g* for 30 min, and the supernatant was assay for protein concentration by amido black quantification as described previously (Li et al., 2012). Protein (100 μg) in solution from each sample was then mixed with equal volume of 2× sample buffer (4% SDS, 125 mM Tris, 20% glycerol, 0.005% bromophenol blue, and 10% mercaptoethanol, pH 6.8) before being separated on a Bio-Rad protean II electrophoresis system with a 4% (v/v) polyacrylamide stacking gel and 12% (v/v) polyacrylamide separation gel. Proteins were visualized by colloidal Coomassie Brilliant Blue G 250 staining.

The SDS-PAGE gel lane for each sample was cut into 12 fractions. The resulting 360 gel pieces were twice decolorized by destain solution (10 mM NH_4NO_3 and 50% acetonitrile) for 45 min. Dried gel pieces from one fraction were digested with 375 ng trypsin at 37°C overnight and then extracted as described previously (Nelson et al., 2014). The digested peptide solutions were dried by vacuum centrifugation at 30°C, resuspended in 20 μL loading

Downloaded from https://academic.oup.com/plcell/article/29/2/207/6099059 by guest on 20 August 2022

buffer (5% acetonitrile and 0.1% formic acid), and filtered by Millipore 0.22-micron filters before being loaded for HPLC separation. A total of 5 μL of filtered samples were loaded onto a C18 high-capacity nano LC chip (Agilent Technologies) using a 1200 series capillary pump (Agilent Technologies) as described previously. Following loading, samples were eluted from the C18 column directly into a 6550 series quadrupole time-of-flight mass spectrometer (Agilent Technologies) with a 1200 series nano pump using the following buffer B (0.1% formic acid in acetonitrile) gradient: 5 to 35% in 35 min, 35 to 95% in 2 min, and 95 to 5% in 1 min. Parameter settings in the mass spectrometer were as described previously (Nelson et al., 2014).

Agilent .d files were converted to mzML using the Msconvert package (version 2.2.2973) from the Proteowizard project, and mzML files were subsequently converted to Mascot generic files using the mzxml2 search tool from the TPPL version 4.6.2. Mascot generic file peak lists were searched against an in-house Arabidopsis database comprising ATH1.pep (release 10) from TAIR and the Arabidopsis mitochondrial and plastid protein sets (33,621 sequences; 13,487,170 residues) (Lamesch et al., 2012) using the Mascot search engine version 2.3 and using error tolerances of 100 ppm for MS and 0.5 D for MS/MS; "max missed cleavages" set to 1; variable modifications of oxidation (Met) and carbamidomethyl (Cys). We used iProphet and ProteinProphet from the Trans Proteomic Pipeline to analyze peptide and protein probability and global FDR (Nesvizhskii et al., 2003; Deutsch et al., 2010; Shteynberg et al., 2011). The reported peptide lists with P = 0.8 have FDRs of <3% and protein lists with P = 0.95 have FDRs of <0.5%. Quantification of LPFs were accomplished by an in-house script written in Mathematica as described previously (Nelson et al., 2014). The data for determination of LPF for peptides by ^{15}N progressive labeling are provided in Supplemental Data Set 14, and the peptide identification data are in Supplemental Data Set 15.

Calculation of K_D and K_S

Protein degradation is a first order and stochastic process, and an exponential rate (K_D) is used to represent the proportional decrease of current protein abundance per day. Protein synthesis is a zero order process and is thus described as a proportional increase of its starting pool (K_S/A) per day (Claydon and Beynon, 2012; Li et al., 2012). "A" is the starting abundance for a specific protein at the beginning of the labeling period (T0). Because of the stochastic nature of degradation, newly synthesized proteins experience the same proportional decrease as existing proteins. As a result, calculation of gross synthesis rates requires the measurement of newly synthesized proteins and the addition of the proportion of newly synthesized proteins lost by degradation. Protein degradation rate K_D and synthesis rate K_S/A for specific proteins were calculated from the progressive labeling data using a combination of FCP and the LPF following a method described previously (Li et al., 2012).

K_D calculation:

$$K_D = -\frac{\ln FCP \cdot (1 - LPF)}{t}$$

K_S calculation:

$$\frac{K_S}{A} = \frac{FCP - e^{-K_D \cdot t}}{1 - e^{-K_D \cdot t}} \cdot K_D$$

The fresh weight of leaves with a protein content correction was first used as an approximate value of fold change in protein abundance (measured FCP), and this was applied to calculate degradation rates (K_D). However, it is challenging to measure FCP and protein turnover simultaneously from the same samples, and sample-to-sample variation in measuring them separately affects the calculation of protein degradation rates. In addition, different leaves were found to show different nitrogen uptake and assimilation capability (Masclaux-Daubresse et al., 2010) and could thus lead to different lag effects in ^{15}N labeling. Younger leaves appeared to show faster nitrogen assimilation rates into amino acid pools compared with relatively older leaves, which is evidenced by the higher ^{15}N enrichment in the same peptide of younger leaves. To avoid these effects on degradation rate calculation and comparisons across leaves, a median polish strategy, which has been widely used for multiple experiment normalization (Lim et al., 2007), was employed to preprocess the data. The median LPF value in each sample is a good indicator of FCP for each experimental replicate. Based on a time point–to–time point protein turnover rate calculation (Li et al., 2012), a calculated FCP for each sample can be deduced (calculated FCP).

$$FCP = \frac{e^{-K_D \cdot t}}{1 - LPF} \quad (t \text{ is equal to } ^{15}N \text{ labelling time})$$

The comparison of calculated FCP and measured FCP showed a strong correlation (k = 1.00, R = 0.95), but calculated FCP recognizes subtle growth changes in individual samples and gives more precise calculations of K_D and K_S values. Calculated FCP was applied for further calculations. Protein degradation comparison of the same protein from leaves 3 and 7 is presented as a relative ΔK_D value [i.e., (L7 K_D–L3 K_D)/average (L3 and 7 K_D)].

Defining Protein Orthologs in Barley

Protein sequences were obtained from MIPS PlantsDB (Nussbaumer et al., 2013) for barley (*Hordeum vulgare*), and orthologs for those proteins with quantified degradation rates in barley (Nelson et al., 2014) were then acquired through BLASTP provided by TAIR release 10. The highest scoring Arabidopsis ortholog was selected for each protein in barley given its E-value was below 10^{-5}. Correlation of protein degradation rates between Arabidopsis and barley was assessed by parametric (Pearson) and nonparametric (Spearman and Kendal) tests.

Energy Cost and Production for Protein Turnover

For a specific protein, energy cost for turnover was calculated to depend upon absolute protein abundance (PA), amino acid length (AAL), protein degradation rate (K_D), and synthesis rate (K_S). Protein degradation cost was based on 1 to 1.5 ATP per residue in the proteasome degradation pathway (Peth et al., 2013). Protein synthesis cost was based on 5 to 5.5 ATP per residue in ribosome translation, protein transport and amino acid biosynthesis (Piques et al., 2009; Kaleta et al., 2013). The energy cost in ATP for degradation and new synthesis of a specific protein was calculated by $1.25 \cdot PA \cdot AAL \cdot K_D / 5.25\ PA \cdot AAL \cdot K_S$ ($\mu mol \cdot d^{-1}$). Whole protein content was measured as fresh weight of leaf tissues (~2% protein per FW). Whole amino acid absolute abundance can be calculated based on whole protein content and average amino acid molecular weight. The gross amino acid residue content of proteins of each leaf number was calculated by averaged values from T0 to 5: leaf 3 (9.59 μmol), leaf 5 (18.69 μmol), leaf 7 (18.97 μmol), and overall (47.24 μmol). Relative protein abundances for the 1228 proteins in ppm were acquired from the Arabidopsis leaves abundance data sets aggregated in the PaxDb database (Piques et al., 2009; Gfeller et al., 2011; Baerenfaller et al., 2012; Wang et al., 2012) with the exception that the numbers for the Rubisco large subunit (RBCL), which is well outside the normal distribution of values in PaxDb, were replaced by a number from experimental evidence, based on the fact that 40% of total soluble protein in Arabidopsis is Rubisco (Eckardt et al., 1997) and that only 50 to 60% of leaf protein is soluble. This means RBCL represents 23.2% of total leaf protein by mass or 16.5% by molar ratio in Arabidopsis, replacing PaxDb numbers for RBCL of 8.8% by mass and 6.6% by molar ratio.

The ATP production rate of respiration is based on experimentally determined respiration rates presented as oxygen consumption 100 $nmol \cdot min^{-1} \cdot g^{-1}$ in different Arabidopsis leaves (Sew et al., 2013). ATP production rates in different leaves can be deduced based on 1 O_2-4.5 ATP: leaf 3 (34.20 $\mu mol \cdot d^{-1}$), leaf 5 (67.05 $\mu mol \cdot d^{-1}$), leaf 7 (69.86 $\mu mol \cdot d^{-1}$),

Downloaded from https://academic.oup.com/plcell/article/29/2/207/6099059 by guest on 20 August 2022

and overall (171.11 $\mu mol \cdot d^{-1}$). Calculations of energy cost and production for protein turnover are detailed in Supplemental Data Set 7A.

Accession Numbers

All accession numbers used are from the TAIR10 annotation of the Arabidopsis genome (www.arabidopsis.org). Raw MS data for ^{15}N progressive labeling can be downloaded via ProteomeXchange: PXD004550. Raw MS data for the relative abundance of proteins between leaves and time points can be downloaded via ProteomeXchange: PXD004549.

Supplemental Data

Supplemental Figure 1. Arabidopsis leaf growth rates and leaf protein content.

Supplemental Figure 2. A flow diagram of tissue sampling and mass spectrometry for ^{15}N progressive labeling and ^{15}N spiked analysis of protein abundance experiments in leaves 3, 5, and 7 of the Arabidopsis rosette over time.

Supplemental Figure 3. Determination of the labeled protein fraction for peptide and protein degradation rate measurements.

Supplemental Figure 4. The ^{15}N enrichment level in the heavy labeled ^{15}N peptide population in each leaf at each time point.

Supplemental Figure 5. The protein degradation (K_D) rates of the 146 proteins that were present in all 27 samples analyzed, before and after the median-polish normalization.

Supplemental Figure 6. A set of 49 degradation rates (K_D) for photosynthesis proteins involved in different protein complexes and functional categories calculated by regression in leaves 3, 5, and 7.

Supplemental Figure 7. The relative protein abundance of CPN60A (At2g28000), HPT108 (At3g63190), and PGK1 (PHOSPHOGLYCERATE KINASE1; At3g12780) in leaves 3, 5, and 7.

The following materials have been deposited in the DRYAD repository under accession number http://dx.doi.org/10.5061/dryad.q3h85.

Supplemental Data Set 1. Growth rates of Arabidopsis leaf 3, leaf 5, and leaf 7.

Supplemental Data Set 2. Protein degradation rates of 1228 proteins and statistical analysis across samples.

Supplemental Data Set 3. Ratios of specific protein abundances relative to a fully^{15}N labeled reference.

Supplemental Data Set 4. The correlation of intrinsic properties of proteins with their protein degradation rates.

Supplemental Data Set 5. Comparison of protein degradation rate (K_D) and protein abundance between selected proteins in leaf 3 and leaf 7.

Supplemental Data Set 6. Comparison of protein degradation rate (K_D) and leaf growth rates in leaf 3, leaf 5, and leaf 7.

Supplemental Data Set 7. Calculation of ATP costs for protein synthesis and degradation in leaf 3, leaf 5, and leaf 7.

Supplemental Data Set 8. Comparison of protein degradation rate and protein abundance for selected proteins of interest.

Supplemental Data Set 9. Determination of protein abundance fold change relative to a ^{15}N reference in 36 individual leaf samples.

Supplemental Data Sets 10 to 13. The peptide identification data for each time point for peptides at T = 0, 1, 3, and 5 d in the spiked in ^{15}N reference experiment, respectively.

Supplemental Data Set 14. Determination of LPF for peptides by ^{15}N progressive labeling in 27 individual leaf samples.

Supplemental Data Set 15. The peptide identification data for ^{15}N progressively labeled peptides at all time points.

ACKNOWLEDGMENTS

This work was supported by the facilities of the Australian Research Council Centre of Excellence Program (CE140100008). A.H.M. was funded by an ARC Future Fellowship (FT110100242).

AUTHOR CONTRIBUTIONS

L.L. performed most of the experiments and data analysis. C.J.N. helped design experiments and advised on and performed some of the mass spectrometry and data analysis. J.T. and I.C. provided computational support and scripts and aided in data analysis. A.H.M., L.L., and S.H. designed experiments and analyzed and discussed results. A.H.M. and L.L. wrote the manuscript. All authors commented on the results and the manuscript.

Received October 4, 2016; revised January 12, 2017; accepted January 30, 2017; published January 30, 2017.

REFERENCES

Apel, W., Schulze, W.X., and Bock, R. (2010). Identification of protein stability determinants in chloroplasts. Plant J. **63:** 636–650.

Araújo, W.L., Tohge, T., Ishizaki, K., Leaver, C.J., and Fernie, A.R. (2011). Protein degradation - an alternative respiratory substrate for stressed plants. Trends Plant Sci. **16:** 489–498.

Armbruster, U., Zühlke, J., Rengstl, B., Kreller, R., Makarenko, E., Rühle, T., Schünemann, D., Jahns, P., Weisshaar, B., Nickelsen, J., and Leister, D. (2010). The Arabidopsis thylakoid protein PAM68 is required for efficient D1 biogenesis and photosystem II assembly. Plant Cell **22:** 3439–3460.

Avci, D., and Lemberg, M.K. (2015). Clipping or extracting: two ways to membrane protein degradation. Trends Cell Biol. **25:** 611–622.

Bachmair, A., Finley, D., and Varshavsky, A. (1986). In vivo half-life of a protein is a function of its amino-terminal residue. Science **234:** 179–186.

Baerenfaller, K., et al. (2012). Systems-based analysis of Arabidopsis leaf growth reveals adaptation to water deficit. Mol. Syst. Biol. **8:** 606.

Bläsing, O.E., Gibon, Y., Günther, M., Höhne, M., Morcuende, R., Osuna, D., Thimm, O., Usadel, B., Scheible, W.R., and Stitt, M. (2005). Sugars and circadian regulation make major contributions to the global regulation of diurnal gene expression in Arabidopsis. Plant Cell **17:** 3257–3281.

Boyes, D.C., Zayed, A.M., Ascenzi, R., McCaskill, A.J., Hoffman, N.E., Davis, K.R., and Görlach, J. (2001). Growth stage-based phenotypic analysis of Arabidopsis: a model for high throughput functional genomics in plants. Plant Cell **13:** 1499–1510.

Cambridge, S.B., Gnad, F., Nguyen, C., Bermejo, J.L., Krüger, M., and Mann, M. (2011). Systems-wide proteomic analysis in mammalian cells reveals conserved, functional protein turnover. J. Proteome Res. **10:** 5275–5284.

Chatterjee, A., Abeydeera, N.D., Bale, S., Pai, P.J., Dorrestein, P.C., Russell, D.H., Ealick, S.E., and Begley, T.P. (2011). *Saccharomyces cerevisiae* THI4p is a suicide thiamine thiazole synthase. Nature **478:** 542–546.

Downloaded from https://academic.oup.com/plcell/article/29/2/207/6099059 by guest on 20 August 2022

Chen, W.P., Yang, X.Y., Harms, G.L., Gray, W.M., Hegeman, A.D., and Cohen, J.D. (2011). An automated growth enclosure for metabolic labeling of Arabidopsis thaliana with 13C-carbon dioxide - an in vivo labeling system for proteomics and metabolomics research. Proteome Sci. **9:** 9.

Christiano, R., Nagaraj, N., Fröhlich, F., and Walther, T.C. (2014). Global proteome turnover analyses of the yeasts *S. cerevisiae* and *S. pombe*. Cell Reports **9:** 1959–1965.

Claydon, A.J., and Beynon, R. (2012). Proteome dynamics: revisiting turnover with a global perspective. Mol. Cell. Proteomics **11:** 1551–1565.

De Baets, G., Reumers, J., Delgado Blanco, J., Dopazo, J., Schymkowitz, J., and Rousseau, F. (2011). An evolutionary trade-off between protein turnover rate and protein aggregation favors a higher aggregation propensity in fast degrading proteins. PLOS Comput. Biol. **7:** e1002090.

Deutsch, E.W., et al. (2010). A guided tour of the Trans-Proteomic Pipeline. Proteomics **10:** 1150–1159.

Doherty, M.K., Hammond, D.E., Clague, M.J., Gaskell, S.J., and Beynon, R.J. (2009). Turnover of the human proteome: determination of protein intracellular stability by dynamic SILAC. J. Proteome Res. **8:** 104–112.

Eckardt, N.A., Snyder, G.W., Portis, A.R., Jr., and Orgen, W.L. (1997). Growth and photosynthesis under high and low irradiance of Arabidopsis thaliana antisense mutants with reduced ribulose-1,5-bisphosphate carboxylase/oxygenase activase content. Plant Physiol. **113:** 575–586.

Edwards, J.M., Roberts, T.H., and Atwell, B.J. (2012). Quantifying ATP turnover in anoxic coleoptiles of rice (Oryza sativa) demonstrates preferential allocation of energy to protein synthesis. J. Exp. Bot. **63:** 4389–4402.

Ellis, R.J. (1981). Chloroplast proteins - synthesis, transport, and assembly. Annu. Rev. Plant Physiol. Plant Mol. Biol. **32:** 111–137.

Fan, K.T., Rendahl, A.K., Chen, W.P., Freund, D.M., Gray, W.M., Cohen, J.D., and Hegeman, A.D. (2016). Proteome scale-protein turnover analysis using high resolution mass spectrometric data from stable-isotope labeled plants. J. Proteome Res. **15:** 851–867.

Fernandez-Escamilla, A.M., Rousseau, F., Schymkowitz, J., and Serrano, L. (2004). Prediction of sequence-dependent and mutational effects on the aggregation of peptides and proteins. Nat. Biotechnol. **22:** 1302–1306.

Fleig, L., Bergbold, N., Sahasrabudhe, P., Geiger, B., Kaltak, L., and Lemberg, M.K. (2012). Ubiquitin-dependent intramembrane rhomboid protease promotes ERAD of membrane proteins. Mol. Cell **47:** 558–569.

Flügge, U.I., Häusler, R.E., Ludewig, F., and Gierth, M. (2011). The role of transporters in supplying energy to plant plastids. J. Exp. Bot. **62:** 2381–2392.

Gfeller, A., Baerenfaller, K., Loscos, J., Chételat, A., Baginsky, S., and Farmer, E.E. (2011). Jasmonate controls polypeptide patterning in undamaged tissue in wounded Arabidopsis leaves. Plant Physiol. **156:** 1797–1807.

Giraud, E., Ng, S., Carrie, C., Duncan, O., Low, J., Lee, C.P., Van Aken, O., Millar, A.H., Murcha, M., and Whelan, J. (2010). TCP transcription factors link the regulation of genes encoding mitochondrial proteins with the circadian clock in *Arabidopsis thaliana*. Plant Cell **22:** 3921–3934.

Gonda, D.K., Bachmair, A., Wünning, I., Tobias, J.W., Lane, W.S., and Varshavsky, A. (1989). Universality and structure of the N-end rule. J. Biol. Chem. **264:** 16700–16712.

Guan, S.H., Price, J.C., Prusiner, S.B., Ghaemmaghami, S., and Burlingame, A.L. (2011). A data processing pipeline for mammalian proteome dynamics studies using stable isotope metabolic labeling. Mol. Cell. Proteomics **10:** M111.010728.

Hasan, S.S., Yamashita, E., Baniulis, D., and Cramer, W.A. (2013). Quinone-dependent proton transfer pathways in the photosynthetic cytochrome b6f complex. Proc. Natl. Acad. Sci. USA **110:** 4297–4302.

Hooper, C.M., Tanz, S.K., Castleden, I.R., Vacher, M.A., Small, I.D., and Millar, A.H. (2014). SUBAcon: a consensus algorithm for unifying the subcellular localization data of the Arabidopsis proteome. Bioinformatics **30:** 3356–3364.

Huang, S., Nelson, C.J., Li, L., Taylor, N.L., Ströher, E., Peteriet, J., and Millar, A.H. (2015). INTERMEDIATE CLEAVAGE PEPTIDASE55 modifies enzyme amino termini and alters protein stability in Arabidopsis mitochondria. Plant Physiol. **168:** 415–427.

Huang, W., Ling, Q., and Jarvis, P. (2013). The ubiquitin-proteasome system regulates chloroplast biogenesis. Commun. Integr. Biol. **6:** e23001.

Ishihara, H., Obata, T., Sulpice, R., Fernie, A.R., and Stitt, M. (2015). Quantifying protein synthesis and degradation in Arabidopsis by dynamic $^{13}CO_2$ labeling and analysis of enrichment in individual amino acids in their free pools and in protein. Plant Physiol. **168:** 74–93.

Janska, H., Kwasniak, M., and Szczepanowska, J. (2013). Protein quality control in organelles - AAA/FtsH story. Biochim. Biophys. Acta **1833:** 381–387.

Juntawong, P., Girke, T., Bazin, J., and Bailey-Serres, J. (2014). Translational dynamics revealed by genome-wide profiling of ribosome footprints in Arabidopsis. Proc. Natl. Acad. Sci. USA **111:** E203–E212.

Kaleta, C., Schäuble, S., Rinas, U., and Schuster, S. (2013). Metabolic costs of amino acid and protein production in *Escherichia coli*. Biotechnol. J. **8:** 1105–1114.

Karunadharma, P.P., Basisty, N., Chiao, Y.A., Dai, D.F., Drake, R., Levy, N., Koh, W.J., Emond, M.J., Kruse, S., Marcinek, D., Maccoss, M.J., and Rabinovitch, P.S. (2015). Respiratory chain protein turnover rates in mice are highly heterogeneous but strikingly conserved across tissues, ages, and treatments. FASEB J. **29:** 3582–3592.

Kato, Y., Sun, X., Zhang, L., and Sakamoto, W. (2012). Cooperative D1 degradation in the photosystem II repair mediated by chloroplastic proteases in Arabidopsis. Plant Physiol. **159:** 1428–1439.

Kramer, D.M., and Evans, J.R. (2011). The importance of energy balance in improving photosynthetic productivity. Plant Physiol. **155:** 70–78.

Lam, M.P., et al. (2014). Protein kinetic signatures of the remodeling heart following isoproterenol stimulation. J. Clin. Invest. **124:** 1734–1744.

Lambreva, M.D., Russo, D., Polticelli, F., Scognamiglio, V., Antonacci, A., Zobnina, V., Campi, G., and Rea, G. (2014). Structure/function/dynamics of photosystem II plastoquinone binding sites. Curr. Protein Pept. Sci. **15:** 285–295.

Lamesch, P., et al. (2012). The Arabidopsis Information Resource (TAIR): improved gene annotation and new tools. Nucleic Acids Res. **40:** D1202–D1210.

Lee, C.P., Eubel, H., and Millar, A.H. (2010). Diurnal changes in mitochondrial function reveal daily optimization of light and dark respiratory metabolism in Arabidopsis. Mol. Cell. Proteomics **9:** 2125–2139.

Li, L., Nelson, C., Fenske, R., Trösch, J., Pružinská, A., Millar, A.H., and Huang, S. (2016). Changes in specific protein degradation rates in Arabidopsis thaliana reveal multiple roles of Lon1 in mitochondrial protein homeostasis. Plant J., 10.1111/tpj.13392.

Li, L., Nelson, C.J., Solheim, C., Whelan, J., and Millar, A.H. (2012). Determining degradation and synthesis rates of arabidopsis proteins using the kinetics of progressive 15N labeling of two-dimensional gel-separated protein spots. Mol. Cell. Proteomics **11:** M111 010025.

Downloaded from https://academic.oup.com/plcell/article/29/2/207/6099059 by guest on 20 August 2022

Liang, C., Cheng, S., Zhang, Y., Sun, Y., Fernie, A.R., Kang, K., Panagiotou, G., Lo, C., and Lim, B.L. (2016). Transcriptomic, proteomic and metabolic changes in Arabidopsis thaliana leaves after the onset of illumination. BMC Plant Biol. **16:** 43.

Lim, W.K., Wang, K., Lefebvre, C., and Califano, A. (2007). Comparative analysis of microarray normalization procedures: effects on reverse engineering gene networks. Bioinformatics **23:** i282–i288.

Ling, Q., Huang, W., Baldwin, A., and Jarvis, P. (2012). Chloroplast biogenesis is regulated by direct action of the ubiquitin-proteasome system. Science **338:** 655–659.

Lyon, D., Castillejo, M.A., Mehmeti-Tershani, V., Staudinger, C., Kleemaier, C., and Wienkoop, S. (2016). Drought and recovery: independently regulated processes highlighting the importance of protein turnover dynamics and translational regulation in *Medicago truncatula*. Mol. Cell. Proteomics **15:** 1921–1937.

Masclaux-Daubresse, C., Daniel-Vedele, F., Dechorgnat, J., Chardon, F., Gaufichon, L., and Suzuki, A. (2010). Nitrogen uptake, assimilation and remobilization in plants: challenges for sustainable and productive agriculture. Ann. Bot. (Lond.) **105:** 1141–1157.

Melis, A. (1999). Photosystem-II damage and repair cycle in chloroplasts: what modulates the rate of photodamage? Trends Plant Sci. **4:** 130–135.

Mockler, T.C., Michael, T.P., Priest, H.D., Shen, R., Sullivan, C.M., Givan, S.A., McEntee, C., Kay, S.A., and Chory, J. (2007). The DIURNAL project: DIURNAL and circadian expression profiling, model-based pattern matching, and promoter analysis. Cold Spring Harb. Symp. Quant. Biol. **72:** 353–363.

Nelson, C.J., Alexova, R., Jacoby, R.P., and Millar, A.H. (2014). Proteins with high turnover rate in barley leaves estimated by proteome analysis combined with in planta isotope labeling. Plant Physiol. **166:** 91–108.

Nelson, C.J., Li, L., Jacoby, R.P., and Millar, A.H. (2013). Degradation rate of mitochondrial proteins in *Arabidopsis thaliana* cells. J. Proteome Res. **12:** 3449–3459.

Nesvizhskii, A.I., Keller, A., Kolker, E., and Aebersold, R. (2003). A statistical model for identifying proteins by tandem mass spectrometry. Anal. Chem. **75:** 4646–4658.

Nishimura, K., Fukagawa, T., Takisawa, H., Kakimoto, T., and Kanemaki, M. (2009). An auxin-based degron system for the rapid depletion of proteins in nonplant cells. Nat. Methods **6:** 917–922.

Nussbaumer, T., Martis, M.M., Roessner, S.K., Pfeifer, M., Bader, K.C., Sharma, S., Gundlach, H., and Spannagl, M. (2013). MIPS PlantsDB: a database framework for comparative plant genome research. Nucleic Acids Res. **41:** D1144–D1151.

Osteryoung, K.W., and Pyke, K.A. (2014). Division and dynamic morphology of plastids. Annu. Rev. Plant Biol. **65:** 443–472.

Peth, A., Nathan, J.A., and Goldberg, A.L. (2013). The ATP costs and time required to degrade ubiquitinated proteins by the 26 S proteasome. J. Biol. Chem. **288:** 29215–29222.

Piques, M., Schulze, W.X., Höhne, M., Usadel, B., Gibon, Y., Rohwer, J., and Stitt, M. (2009). Ribosome and transcript copy numbers, polysome occupancy and enzyme dynamics in Arabidopsis. Mol. Syst. Biol. **5:** 314.

Ponnala, L., Wang, Y., Sun, Q., and van Wijk, K.J. (2014). Correlation of mRNA and protein abundance in the developing maize leaf. Plant J. **78:** 424–440.

Price, J.C., Guan, S., Burlingame, A., Prusiner, S.B., and Ghaemmaghami, S. (2010). Analysis of proteome dynamics in the mouse brain. Proc. Natl. Acad. Sci. USA **107:** 14508–14513.

Reinhold, T., Alawady, A., Grimm, B., Beran, K.C., Jahns, P., Conrath, U., Bauer, J., Reiser, J., Melzer, M., Jeblick, W., and Neuhaus, H.E. (2007). Limitation of nocturnal import of ATP into Arabidopsis chloroplasts leads to photooxidative damage. Plant J. **50:** 293–304.

Ren, M., Qiu, S., Venglat, P., Xiang, D., Feng, L., Selvaraj, G., and Datla, R. (2011). Target of rapamycin regulates development and ribosomal RNA expression through kinase domain in Arabidopsis. Plant Physiol. **155:** 1367–1382.

Rousseeuw, P.J. (1987). Silhouettes: A graphical aid to the interpretation and validation of cluster analysis. J. Comput. Appl. Math. **20:** 53–65.

Rowland, E., Kim, J., Bhuiyan, N.H., and van Wijk, K.J. (2015). The Arabidopsis chloroplast stromal N-terminome: Complexities of amino-terminal protein maturation and stability. Plant Physiol. **169:** 1881–1896.

Scheurwater, I., Dünnebacke, M., Eising, R., and Lambers, H. (2000). Respiratory costs and rate of protein turnover in the roots of a fast-growing (*Dactylis glomerata* L.) and a slow-growing (*Festuca ovina* L.) grass species. J. Exp. Bot. **51:** 1089–1097.

Schmitz, G., Reinhold, T., Göbel, C., Feussner, I., Neuhaus, H.E., and Conrath, U. (2010). Limitation of nocturnal ATP import into chloroplasts seems to affect hormonal crosstalk, prime defense, and enhance disease resistance in *Arabidopsis thaliana*. Mol. Plant Microbe Interact. **23:** 1584–1591.

Schmitz, J., Heinrichs, L., Scossa, F., Fernie, A.R., Oelze, M.L., Dietz, K.J., Rothbart, M., Grimm, B., Flügge, U.I., and Häusler, R.E. (2014). The essential role of sugar metabolism in the acclimation response of *Arabidopsis thaliana* to high light intensities. J. Exp. Bot. **65:** 1619–1636.

Schwanhäusser, B., Busse, D., Li, N., Dittmar, G., Schuchhardt, J., Wolf, J., Chen, W., and Selbach, M. (2011). Global quantification of mammalian gene expression control. Nature **473:** 337–342.

Sew, Y.S., Ströher, E., Holzmann, C., Huang, S., Taylor, N.L., Jordana, X., and Millar, A.H. (2013). Multiplex micro-respiratory measurements of Arabidopsis tissues. New Phytol. **200:** 922–932.

Shteynberg, D., Deutsch, E.W., Lam, H., Eng, J.K., Sun, Z., Tasman, N., Mendoza, L., Moritz, R.L., Aebersold, R., and Nesvizhskii, A.I. (2011). iProphet: multi-level integrative analysis of shotgun proteomic data improves peptide and protein identification rates and error estimates. Mol. Cell. Proteomics **10:** M111 007690.

Siddell, S.G., and Ellis, R.J. (1975). Protein synthesis in chloroplasts. Characteristics and products of protein synthesis in vitro in etioplasts and developing chloroplasts from pea leaves. Biochem. J. **146:** 675–685.

Smith, S.M., Fulton, D.C., Chia, T., Thorneycroft, D., Chapple, A., Dunstan, H., Hylton, C., Zeeman, S.C., and Smith, A.M. (2004). Diurnal changes in the transcriptome encoding enzymes of starch metabolism provide evidence for both transcriptional and post-transcriptional regulation of starch metabolism in Arabidopsis leaves. Plant Physiol. **136:** 2687–2699.

Suzuki, K., Nakanishi, H., Bower, J., Yoder, D.W., Osteryoung, K.W., and Miyagishima, S.Y. (2009). Plastid chaperonin proteins Cpn60 alpha and Cpn60 beta are required for plastid division in *Arabidopsis thaliana*. BMC Plant Biol. **9:** 38.

Takahashi, S., and Badger, M.R. (2011). Photoprotection in plants: a new light on photosystem II damage. Trends Plant Sci. **16:** 53–60.

Tanz, S.K., Castleden, I., Hooper, C.M., Vacher, M., Small, I., and Millar, H.A. (2013). SUBA3: a database for integrating experimentation and prediction to define the SUBcellular location of proteins in Arabidopsis. Nucleic Acids Res. **41:** D1185–D1191.

Umena, Y., Kawakami, K., Shen, J.R., and Kamiya, N. (2011). Crystal structure of oxygen-evolving photosystem II at a resolution of 1.9 Å. Nature **473:** 55–60.

van Wijk, K.J. (2015). Protein maturation and proteolysis in plant plastids, mitochondria, and peroxisomes. Annu. Rev. Plant Biol. **66:** 75–111.

Vierstra, R.D. (2009). The ubiquitin-26S proteasome system at the nexus of plant biology. Nat. Rev. Mol. Cell Biol. **10:** 385–397.

Downloaded from https://academic.oup.com/plcell/article/29/2/207/6099059 by guest on 20 August 2022

Vögtle, F.N., Wortelkamp, S., Zahedi, R.P., Becker, D., Leidhold, C., Gevaert, K., Kellermann, J., Voos, W., Sickmann, A., Pfanner, N., and Meisinger, C. (2009). Global analysis of the mitochondrial N-proteome identifies a processing peptidase critical for protein stability. Cell **139:** 428–439.

Walsh, C.T. (1984). Suicide substrates, mechanism-based enzyme inactivators: recent developments. Annu. Rev. Biochem. **53:** 493–535.

Wang, D., and Portis, A.R., Jr. (2007). A novel nucleus-encoded chloroplast protein, PIFI, is involved in NAD(P)H dehydrogenase complex-mediated chlororespiratory electron transport in Arabidopsis. Plant Physiol. **144:** 1742–1752.

Wang, M., Weiss, M., Simonovic, M., Haertinger, G., Schrimpf, S.P., Hengartner, M.O., and von Mering, C. (2012). PaxDb, a database of protein abundance averages across all three domains of life. Mol. Cell. Proteomics **11:** 492–500.

Waters, M.T., Nelson, D.C., Scaffidi, A., Flematti, G.R., Sun, Y.K., Dixon, K.W., and Smith, S.M. (2012). Specialisation within the DWARF14 protein family confers distinct responses to karrikins and strigolactones in Arabidopsis. Development **139:** 1285–1295.

Wei, X., Su, X., Cao, P., Liu, X., Chang, W., Li, M., Zhang, X., and Liu, Z. (2016). Structure of spinach photosystem II-LHCII supercomplex at 3.2 Å resolution. Nature **534:** 69–74.

Woodson, J.D., Joens, M.S., Sinson, A.B., Gilkerson, J., Salomé, P.A., Weigel, D., Fitzpatrick, J.A., and Chory, J. (2015). Ubiquitin facilitates a quality-control pathway that removes damaged chloroplasts. Science **350:** 450–454.

Yang, X.Y., Chen, W.P., Rendahl, A.K., Hegeman, A.D., Gray, W.M., and Cohen, J.D. (2010). Measuring the turnover rates of Arabidopsis proteins using deuterium oxide: an auxin signaling case study. Plant J. **63:** 680–695.

Yip, C.Y., Harbour, M.E., Jayawardena, K., Fearnley, I.M., and Sazanov, L.A. (2011). Evolution of respiratory complex I: "supernumerary" subunits are present in the alpha-proteobacterial enzyme. J. Biol. Chem. **286:** 5023–5033.

Zaltsman, A., Feder, A., and Adam, Z. (2005). Developmental and light effects on the accumulation of FtsH protease in Arabidopsis chloroplasts–implications for thylakoid formation and photosystem II maintenance. Plant J. **42:** 609–617.

Zhang, H., and Cramer, W.A. (2004). Purification and crystallization of the cytochrome b6f complex in oxygenic photosynthesis. Methods Mol. Biol. **274:** 67–78.

Zhang, H., Deery, M.J., Gannon, L., Powers, S.J., Lilley, K.S., and Theodoulou, F.L. (2015). Quantitative proteomics analysis of the Arg/N-end rule pathway of targeted degradation in Arabidopsis roots. Proteomics **15:** 2447–2457.

Downloaded from https://academic.oup.com/plcell/article/29/2/207/6099059 by guest on 20 August 2022